

**Key Points:**

- Topographic evolution constrained by structural, geomorphic and river analysis of the Pollino range and surrounding extensional basins
- At short spatial scale, increase in rock uplift and fault activity controls the endorheic-exorheic transition
- At regional scale, uplift increases between 400 and 800 ka, due to progressive lateral slab tearing, and inflow asthenospheric mantle

**Supporting Information:**

Supporting Information may be found in the online version of this article.

**Correspondence to:**

R. Clementucci,  
[rclementucci@ethz.ch](mailto:rclementucci@ethz.ch)

**Citation:**

Clementucci, R., Lanari, R., Faccenna, C., Crosetto, S., Reitano, R., Zoppis, G., & Ballato, P. (2024). Morpho-tectonic evolution of the Southern Apennines and Calabrian Arc: Insights from Pollino range and surrounding extensional intermontane basins. *Tectonics*, 43, e2023TC008002. <https://doi.org/10.1029/2023TC008002>

Received 6 JULY 2023

Accepted 7 APR 2024







**Author Contributions:**

**Conceptualization:** R. Clementucci, R. Lanari, C. Faccenna, G. Zoppis  
**Data curation:** R. Clementucci, R. Lanari, S. Crosetto, G. Zoppis  
**Formal analysis:** R. Clementucci, R. Lanari, S. Crosetto, G. Zoppis  
**Funding acquisition:** C. Faccenna  
**Investigation:** R. Clementucci, R. Lanari, C. Faccenna, G. Zoppis  
**Methodology:** R. Clementucci, R. Lanari, S. Crosetto, G. Zoppis  
**Project administration:** C. Faccenna  
**Resources:** R. Clementucci, R. Lanari, S. Crosetto, G. Zoppis  
**Software:** R. Clementucci, R. Lanari, G. Zoppis

© 2024 The Authors.

This is an open access article under the terms of the [Creative Commons Attribution-NonCommercial License](https://creativecommons.org/licenses/by-nc/4.0/), which permits use, distribution and reproduction in any medium, provided the original work is properly cited and is not used for commercial purposes.

## Morpho-Tectonic Evolution of the Southern Apennines and Calabrian Arc: Insights From Pollino Range and Surrounding Extensional Intermontane Basins

R. Clementucci<sup>1,2</sup> , R. Lanari<sup>1,3</sup> , C. Faccenna<sup>1,4</sup> , S. Crosetto<sup>4</sup> , R. Reitano<sup>1</sup> , G. Zoppis<sup>1</sup>, and P. Ballato<sup>1</sup> 

<sup>1</sup>Dipartimento di Scienze, Università Roma Tre, Rome, Italy, <sup>2</sup>Department of Earth Sciences, ETH Zürich, Zürich, Switzerland, <sup>3</sup>Institute of Geosciences and Earth Resources, National Research Council of Italy (CNR), Florence, Italy, <sup>4</sup>GFZ-German Research Centre for Geosciences, Potsdam, Germany

**Abstract** The evolution of topography in forearc regions results from the complex interplay of crustal and mantle processes. The Southern Apennines represent a well-studied forearc region that experienced several tectonic phases, initially marked by compressional deformation followed by extension and large-scale uplift. We present a new structural, geomorphic and fluvial analysis of the Pollino Massif and surrounding intermontane basins (Mercure, Campotenesse and Castrovallari) to unravel their evolution since the Pliocene. We constrain multiple tectonic transport directions, evolution of the drainage, and magnitude and timing of long-term incision following base level falls. Two sets of knickpoints suggest two phases of base level lowering and allow to estimate ~500 m of long-term uplift (late Pleistocene), as observed in the Sila Massif. On a smaller spatial scale, the evolution and formation of topographic relief, sedimentation, and opening of intermontane basins is strongly controlled by the recent increase in rock uplift rate and fault activity. At the regional scale, an along-strike, long-wavelength uplift pattern from north to south can be explained by progressive lateral slab tearing and inflow of asthenospheric mantle beneath Pollino and Sila, which in turn may have promoted extensional tectonics. The lower uplift of Le Serre Massif may be explained as result of weak plate coupling due to narrowing of the Calabrian slab. The onset of uplift in the Pollino Massif, ranging from 400 to 800 ka, is consistent with that one proposed in the southern Calabrian forearc, suggesting a possible synchronism of uplift, and lateral tearing of the Calabrian slab.

### 1. Introduction

The origin and evolution of topography in mountain belts result from the feedback between crustal tectonics, mantle dynamics, and surface processes. However, due to the interaction and superimposition of shallow and deep mechanisms, identifying the different contributions of processes acting at different temporal and spatial scales may be extremely complex (Cramer et al., 2017; Faccenna & Becker, 2020; Royden, 1993; Wortel & Spakman, 2000).

At convergent plate boundaries, crustal underplating and shallow accretion are considered as the main mechanisms leading to surface uplift and producing an isostatically compensated topography (Beaumont et al., 2000; Willett et al., 2001). Yet subduction processes can cause both positive and negative topography (Duretz & Gerya, 2013). For instance, slab pull may produce negative topography on the forearc and backarc (Cramer et al., 2017; Royden, 1993), but can be counterbalanced by crustal accretion and underplating, which promote surface uplift and building of topographic relief (Willett et al., 2001). When slab break-off occurs, those slab pull forces are released, resulting in large scale uplift (Buiter et al., 2002; Duretz & Gerya, 2013). In such context, a reconstruction of the surface morphology evolution, obtained through the investigation of the topographic wavelength and rate of surface processes, is a fundamental step to understand the dynamics of a subduction system. More specifically, quantifying the relief denudation, exhumation and detecting the different geomorphic features at the surface may help to decipher the processes at depth (topographic wavelength >100 km; Willett et al., 2001).

The Southern Apennines of Italy are an ideal case study for deciphering the mutual influence between crustal and deep processes in a forearc setting. The mountain range is located at the transition between active subduction of the Calabrian arc and the Central Apennines, where slab is completely or partially detached (Lanari, Reitano,

**Supervision:** R. Clementucci, C. Faccenna, R. Reitano, P. Ballato  
**Validation:** R. Clementucci, R. Lanari, C. Faccenna, G. Zoppis  
**Visualization:** R. Clementucci, R. Reitano, P. Ballato  
**Writing – original draft:** R. Clementucci  
**Writing – review & editing:** R. Clementucci, R. Lanari, C. Faccenna, S. Crosetto, R. Reitano, P. Ballato

et al., 2023; Maesano et al., 2017; Wortel & Spakman, 2000). Here, a combination of crustal shortening, recent extensional tectonic activity and large-scale regional uplift resulted in the complex topography of the Pollino range (Brozzetti et al., 2017a; Cowie et al., 2017; Faure Walker et al., 2012; Ferranti et al., 2006; Roda-Boluda & Whittaker, 2017; Schiattarella et al., 2003). However, the active geodynamic processes shaping the Southern Apennines-Calabria are still under discussion, and several contrasting models have been proposed, from active subduction causing underplating in the forearc (Minelli & Faccenna, 2010), to delamination or slab break-off and slab edge upwelling (Ascione et al., 2012; Civello & Margheriti, 2004; Cucci, 2004; Faccenna et al., 2011; Guillaume et al., 2010; Palano et al., 2017; Wortel & Spakman, 2000).

Previous works describe the presence of high-standing fluvial and marine terraces, and attempt to constrain the landscape evolution of the different morpho-structural domains of the Southern Apennines (Caputo et al., 2010; Cerrone et al., 2021; Ferranti et al., 2006; Robustelli et al., 2014; Santoro et al., 2009; Molin et al., 2002). Overlaying to the regional signal, crustal processes control the evolution of relief and intermontane basins at smaller spatial scale (Brozzetti et al., 2017a; Gioia et al., 2011, 2023; Robustelli et al., 2014; Schiattarella et al., 1994). In this context, the link between topographic signal, drainage system and deep mechanisms is still not well-defined, especially due to the difficulty of deciphering the contributions from both deep and shallow processes, which are often coeval. We perform a structural and geomorphic analysis to decipher the topographic evolution of the Southern Apennines since the Pliocene. We focus on the Pollino range and surrounding regions, including the Castrovillari, the Mercure and the Campotenese basins, which represent key areas to constrain the topographic and uplift history at both spatial and temporal scales. In particular, we investigate the Pliocene-Quaternary topographic and crustal evolution of the range in connection with the Sila Massif, proposing a model that may explain the concurrence of extensional tectonics and large-scale topographic uplift over the Calabrian subduction zone.

## 2. Geological Setting

### 2.1. Tectonic Setting

The Southern Apennines represent an orogenic-scale duplex system with an overall eastward vergence induced by the westward subduction of the Adria Plate (Corrado et al., 2005; Mazzoli et al., 2008; Patacca & Scandone, 2007). The structural edifice is composed of Meso-Cenozoic allochthonous (i.e., rootless) units derived from the internal (i.e., western) paleogeographic domains that overlay the Apulian Platform. The roof of this large-scale duplex, from the highest, more internal to the lowest, more external units, consists of: (a) ophiolites and associated deep-marine sediments of the Ligurian and Sicilidi, locally presenting high-pressure metamorphism; (b) shallow-water marine deposits of the Apenninic Platform; and (c) basinal, deep-marine to slope deposits of the Lagonegro, Molise and Sannio nappes (e.g., Liberi & Piluso, 2009; Ogniben, 1969; Patacca & Scandone, 2007). The autochthonous Apulian Platform represents the lowermost units of the duplex system and the orogenic foreland, and consists of a thick Meso-Cenozoic shallow-water carbonate succession, stratigraphically overlain by younger continental deposits (Catalano et al., 2004; Monaco et al., 1998; Ogniben, 1969). This structural architecture implies significant imbrication and telescopic shortening of the external allochthonous sheets which, based on the age of the well-preserved thrust-sheet-top deposits, reached their current location during the early-middle Pleistocene (Ascione et al., 2012; Bonardi et al., 2001; Patacca et al., 1990; Patacca & Scandone, 2007; Tropeano et al., 2002).

While the Southern Apennines include continental units derived from the margin of the Adria plate, the Calabrian arc consists of units belonging to the former southern European/Iberian margin (e.g., Bigi et al., 1989; Carminati et al., 2012; Siravo et al., 2022; Van Dijk et al., 2000). The narrow Calabrian orogenic belt (<100 km) comprises: (a) a pile of broadly east-verging nappes of Hercynian metamorphic and crystalline basement rocks locally covered by Meso-Cenozoic deep-marine sediments (e.g., Santantonio et al., 2016); and (b) an Alpine ophiolitic metamorphic complex (Rossetti et al., 2001). The rocks of both domains show different degrees of Tertiary metamorphism ranging from low grade to high-pressure low-temperature conditions (Molli et al., 2020 and references therein). The exhumation of this nappe stack started in the Oligocene during coeval contractional deformation (top to the E) and extension (top to the W) in eastern and western Calabria, respectively, and continued throughout the early Miocene (Mattei et al., 1999; Olivetti et al., 2017; Rossetti et al., 2001; Vignaroli et al., 2012). Thereafter, widespread regional subsidence led to the deposition of unconformable late Serravallian to Pleistocene, mostly marine, siliciclastic deposits, subsequently cut by normal faults (Corbi et al., 2009; Molin

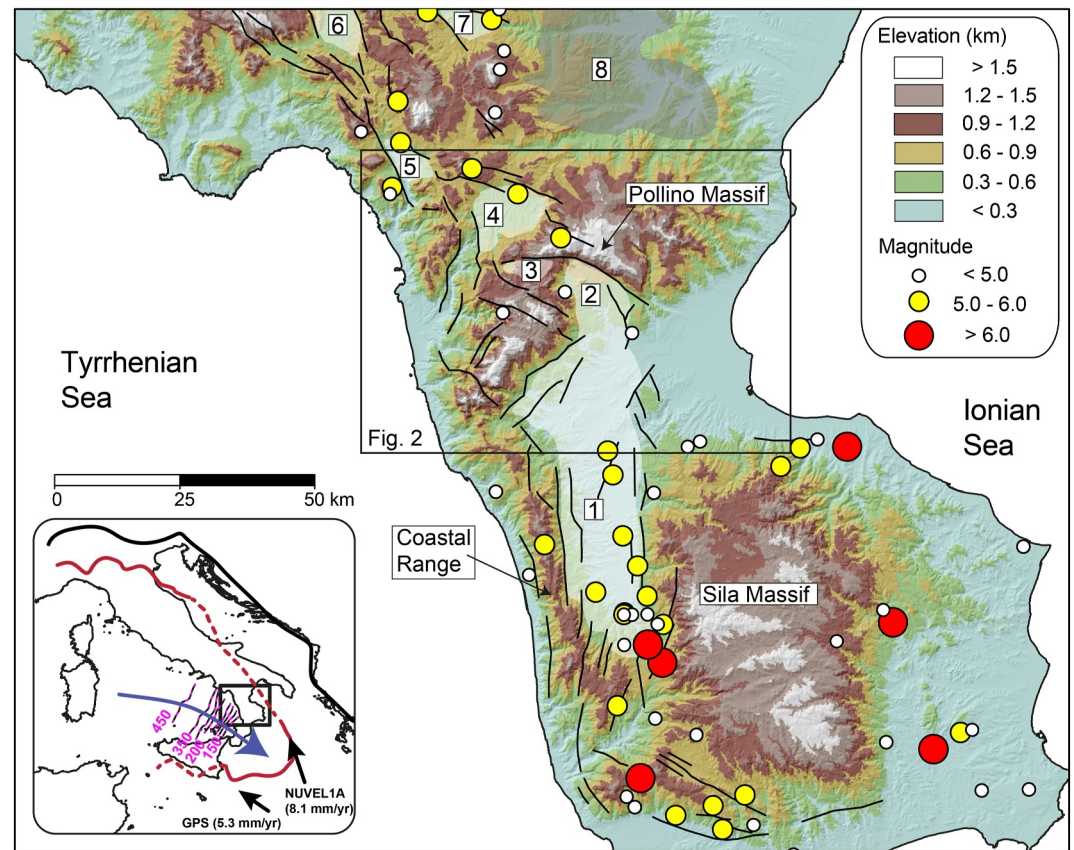


**Figure 1.** Digital elevation model of southern Italy (SRTM DEM, pixel size 90 m), with Quaternary normal faults and associated syn-sedimentary basins (after Brozzetti et al., 2017a). Note, the Sila Massif and the Coastal Range belong to the Calabrian Arc while the Pollino Massif and adjacent mountain ranges are part of the Southern Apennines. Colored dots are the major historical and instrumental earthquakes ( $M_w \geq 4.0$  from 1000 to 2020; CPTI11, Rovida et al., 2011). Extensional intermontane basins: (1) Crati; (2) Castrovillari; (3) Campotenese; (4) Mercure; (5) Noce; (6) Vallo di Diano; (7) Val d'Agri. Wedge-top basin: (8) Sant'Arcangelo. The inset shows the general tectonic setting with the convergence vectors from GPS pole of rotation and Nuvel1A model between Nubia and Eurasia. The colored contour lines represent the depth of the subducted slab and the blue arrow is the trajectory of the Ionian slab (D'Agostino & Selvaggi, 2004).

et al., 2004). The eastward motion of the Calabrian arc started in the late Miocene due to trench retreat and rollback of the Ionian oceanic lithosphere in association with the opening of the Southern Tyrrhenian Basin (e.g., Cifelli et al., 2007; Mattei et al., 1999, 2007). This led to the lateral juxtaposition of the Calabrian arc and the Southern Apennines, most likely from the Pleistocene onward (e.g., Bonardi et al., 2001; Faccenna et al., 2004; Malinverno & Ryan, 1986).

In the study area, mountain building processes were associated with the activity of WNW-ESE-striking, regional, left-lateral strike-slip faults until the late Pliocene—early Pleistocene (Brozzetti et al., 2017a; Catalano et al., 1993, 2004; Dijk et al., 2000; Ferranti et al., 2009; Monaco et al., 1998; Schiattarella, 1998), and later superseded by a more recent NE–SW-oriented direction of extension (Brozzetti et al., 2017a, 2017b; Schiattarella, 1998; Schiattarella et al., 2003). The recent morpho-structural and sedimentary evolution of the Southern Apennines is controlled by the activity of NW-SE-striking normal-oblique fault systems, making the Pollino region one of the most active and seismogenic sectors of the Apennines, despite the seismic gap observed in the historical record (Figure 1; Brozzetti et al., 2017a; Robustelli et al., 2014). The high-angle active and seismogenic normal faults are usually located along the south-western flank of the Pollino, Lauria and La Fagosa Massifs and formed topographic depressions and intermontane basins on the hanging-wall of the structural blocks (Figures 1 and 2). One of these depressions includes the Mercure basin, which consists of an at least 300-m-thick fluvio-lacustrine sedimentary succession recording deposition during glacial-interglacial climate cycles (Figure 3; GE.MI.NA, 1963;

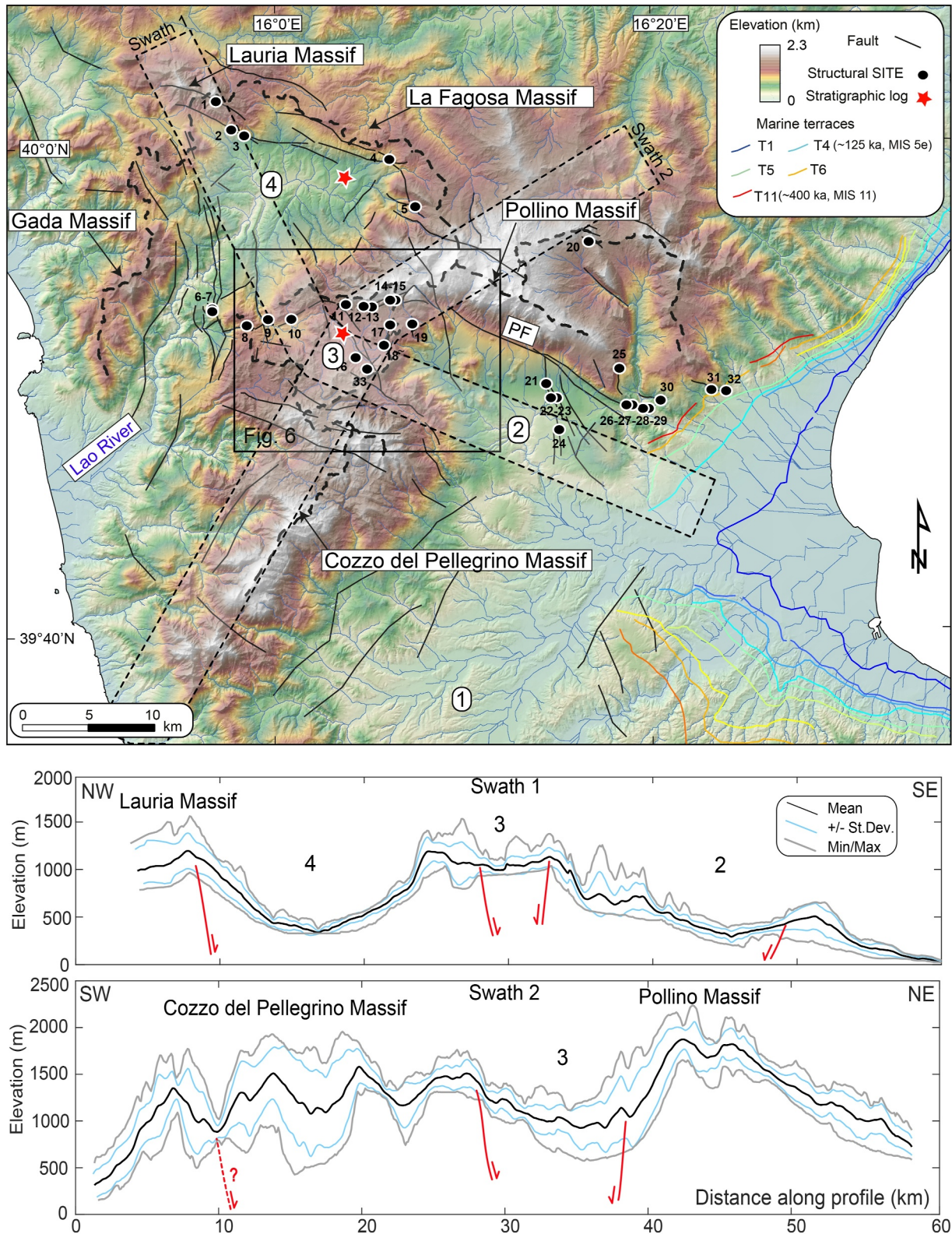


**Figure 2.** Digital elevation model of southern Italy (TINITALY/01 DEM, pixel size 10 m), with Quaternary normal faults (black thin lines) and Middle Pleistocene–Holocene marine terraces on the Ionian coast of northern Calabria (colored lines after Cucci, 2004; Santoro et al., 2009). PF: Pollino Fault. Swath profiles 1 and 2 show the maximum, mean, minimum and standard deviation of elevations of the study area (window 5 km wide). Dashed black lines are the local drainage divide. (1) Crati basin; (2) Castrovillari basin; (3) Campotenese basin; (4) Mercure basin.

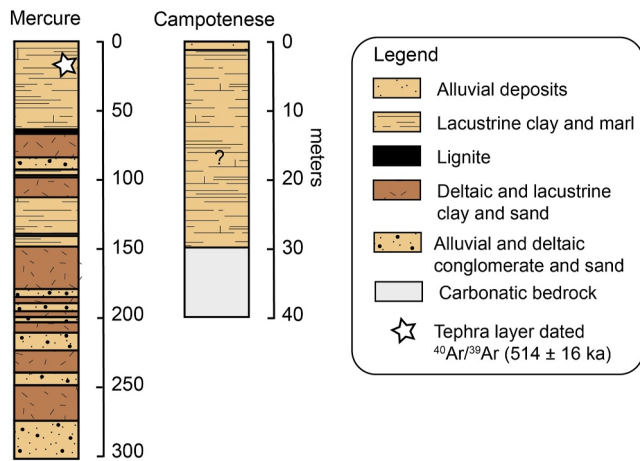


**Figure 3.** Stratigraphic log and borehole data in the Mercure and Campotenese basins, respectively (after Brozzetti et al., 2017a; Robustelli et al., 2014; locations in Figure 2).

Schiattarella et al., 1994; Robustelli et al., 2014). In particular, the base of the sedimentary sequence may range between 1.07 and 0.7 Ma, as suggested by the source area of Castronuovo conglomerates in the Sant’Arcangelo basin attributable to the Apennine platform units located further southwest than the present day drainage divide (Capalbo et al., 2010). The lacustrine sediment at the top of the sequence marks the last phase of evolution of the basin with the endorheic-exorheic transition at 0.5 Ma (Figure 3; Robustelli et al., 2014). A fluvio-lacustrine infill is also found in the smaller Campotenese basin, although the lack of significant fluvial incision and borehole data limits our knowledge on its stratigraphic characteristics (Figure 3; Brozzetti et al., 2017a).

## 2.2. Morphological Setting

The study area is characterized by morpho-structural highs (e.g., Pollino Massif), high-standing erosional surfaces dissected by fluvial incision and Quaternary intermontane basins (e.g., Mercure, Campotenese among others; Figure 1; Brozzetti et al., 2017a; Robustelli et al., 2014).

A series of flat erosional surfaces from 600 to 1,400 m a.s.l. have been described by Robustelli et al. (2014) and Gioia et al. (2011) in the Mercure and Auletta basins, with the highest planation erosional surface associated with a pre-Quaternary uplift stage predating a previous left-lateral tectonic phase and the most recent topographic rejuvenation (Amato & Cinque, 1999; Schiattarella et al., 2003, 2017). During the Quaternary, such regional surfaces are displaced first by strike-slip faults and afterward by the most recent extensional tectonics, which reactivated pre-existing structures (Brozzetti et al., 2017a; Schiattarella, 1998; Schiattarella et al., 2003), and favored the development of intermontane basins (Brozzetti et al., 2017a; Gioia et al., 2011; Robustelli et al., 2014). Similarly, the Sila Massif, Le Serre and the Aspromonte Mountains show a sharp variation in topographic relief and slope consistent with a pattern of river knickpoints, reflecting the transient response of streams to a relative base level change caused by regional uplift and crustal faulting (Olivetti et al., 2012; Roda-Boluda et al., 2019; Roda-Boluda & Whitaker, 2017). Along the Ionian coast, terraces are raised up to several hundred meters above sea level, indicating late Pleistocene uplift (Cucci, 2004; Molin et al., 2002; Santoro et al., 2009). Terrace staircases with more than eleven marine terraces are mapped and laterally correlated across the whole Sibari plain (Figure 2). The lateral correlation is performed between terraces located at similar elevations and displaying analog diagnostic sedimentary features (Santoro et al., 2009). However, in some cases only deeply incised remnants of terrace platforms are found, and the available ages (summarized in Figure S1 in Supporting Information S1) are frequently inconsistent, possibly because of multiple sedimentation and fossil reworking (Nalin et al., 2020; Santoro et al., 2009). For this reason, we will only rely on the terraces attributed to the last interglacial (MIS 5e), which is characterized by the distinctive Senegalese fauna (Santoro et al., 2009). The MIS 5e terrace is the most prominent paleo-shoreline marker and provides an indication of regional uplift of up to 1 mm/yr in the last ~124 Myr (Carobene, 2003; Cucci, 2004; Santoro et al., 2009). Since the terrace is found at progressively lower elevations moving southward from the Pollino to Le Serre Massif, it has previously been suggested that this variation could reflect a spatial variation in uplift rates (Faccenna et al., 2011). However, while direct age-dating for the MIS 5e terrace is available in correspondence of the Pollino and Sila Massifs (Nalin et al., 2020; Santoro et al., 2009), its identification near Le Serre Massif is based only on geometrical cross-correlation (Cerrone et al., 2021; Cucci & Cinti, 1998).

## 3. Methods

### 3.1. Structural Analysis

We carried out a structural analysis to define the geometry, kinematics and, where possible, timing of activity of the main faults (based on morphologic and cross-cutting faulting relationships). The field survey was conducted using available geological maps of the Southern Apennines at different scales and focused on the main structural features. We systematically measured the faults strike and dip, the rake or azimuth of the slickenlines and the sense of shear along the main faults and shear zones. We adopted common criteria to define fault kinematics, such

as lunate and S/C structures, Riedel shears, calcite steps, bedding drag along faults and offset of geological markers (Petit, 1987). In the case of multiple families of slickenlines, cross-cutting relationships were used to determine their relative chronology. To distinguish between potential different slickenline populations, the tectonic transport directions have been attributed after countouring the frequency azimuth of the measured slip direction (Figure S2 in Supporting Information S1). We collected data preferentially on the faults bordering the basins directly with a clear morphological expression, to unambiguously obtain information on the most recent tectonic activity. On the map in Figure 2 we present the site of measurement, while in the supplementary material (Figure S2 and Table S1 in Supporting Information S1) we show a list of structural data with their plots and analyses obtained using the Daisy software (Salvini, 2004).

Our structural analysis can be compared with the large amount of previous works presenting similar analysis along different portions of the investigated area. This is the case of structural surveys in the Mercure (e.g., Brozzetti et al., 2009; Filice & Seeber, 2019) and Castrovillari Basins (e.g., Brozzetti et al., 2017a; Cirillo et al., 2022; Ferranti et al., 2009), in the southern sector of the Pollino range (Ferranti et al., 2009), or at the scale of the Southern Apennines (e.g., Lavecchia et al., 2024; Papanikolaou & Roberts, 2007). It is worth noting that those previous works provide different scenarios, including purely extensional tectonics to transition system from extensional to compressional or left-lateral/extensional regimes.

### 3.2. Topographic Analysis

To investigate the topography and the main tectonic lineaments, we produced topographic slope and local relief maps and performed a regional topographic analysis. Topographic and morphometric maps were obtained in ArcGIS using the Spatial Analyst Toolbox. Local relief was calculated by arithmetically subtracting the maximum and minimum topographic elevations within a circular moving window of 2.5 km. We used a Shuttle Radar Topography Mission Digital Elevation Model (SRTM DEM, pixel size of 90 m; <http://srtm.csi.cgiar.org>) to conduct the regional scale topographic analysis and TINITALY/01, with a spatial resolution of 10 m (Tarquini et al., 2012; data source <http://tinality.pi.ingv.it/download.html>) to perform a detailed analysis of the stream profiles, topography and knickpoints.

### 3.3. Stream Profiles and Knickpoint Analysis

The fluvial network and its channel gradient is highly controlled by climate, bedrock erodibility, and local and regional vertical movements (Kirby & Whipple, 2012).

The slope of longitudinal river profiles under steady-state conditions, when erosion and rock uplift rates are balanced (Flint, 1974; Kirby & Whipple, 2012), is well-described by a power law relationship, known as Flint's Law. Assuming that river channels erode following a shear-stress based power law dependent on discharge (drainage area) and channel slope (Hack, 1957; Morisawa, 1962), and that the river are subjected to steady-state conditions, we can rearrange the Flint's Law as:

$$S = \left(\frac{U}{K}\right)^{\frac{1}{n}} A^{-\left(\frac{\theta}{n}\right)} \quad (1)$$

where  $(U/K)^{1/n}$  and  $m/n$  are the channel steepness index ( $k_s$ ),  $\theta$  is the concavity index, and A the drainage area, respectively (Flint, 1974). In particular, under steady-state conditions and assuming  $n = 1$ ,  $k_s$  (with dimension  $m^{2\theta}$ ) is linearly proportional to the ratio between rock uplift rate ( $U$ ; mm/yr) and bedrock erodibility ( $K$ ;  $m^{1-2m}/yr$ ).  $\theta$  is the concavity index function of  $m$  and  $n$ , which are constants that depend on basin hydrology, channel geometry, and erosion processes (Whipple & Tucker, 1999). The Equation 1 is valid above a critical upstream drainage area of 0.1–5  $km^2$ , where fluvial processes dominate over debris flows (Montgomery & Foufoula-Georgiou, 1993; Wobus et al., 2006). In natural channels, theoretical and empirical studies demonstrated that  $\theta$  usually falls within a relatively restricted range of values between 0.4 and 0.6 (Kirby & Whipple, 2012 and reference therein). To compare  $k_s$  between rivers with greatly differing drainage areas, we calculated the normalized value of channel steepness of the studied rivers ( $k_{sn}$ ) by using a reference concavity index ( $\theta_{ref}$ ) of 0.45. The channels and knickpoints were analyzed using the integral approach, which accounts for the integration of Equation 1, and assuming spatially invariant uplift and erodibility (Perron & Royden, 2013):

$$z(x) = z(x_b) + k_s A_0^{-\frac{m}{n}} \chi \quad (2)$$

where

$$\chi = \int_{x_b}^x \left( \frac{A_0}{A(x')} \right)^{\frac{m}{n}} dx \quad (3)$$

and  $z(x)$  and  $z(x_b)$  are the elevation along the channel profile at distance  $x$  and at the base level ( $x_b$ ), respectively, and  $A_0$  is the reference drainage area (Perron & Royden, 2013). The  $\chi$  approach allows us to visualize  $k_{sn}$  variation along stream segments, revealing possible knickpoints, which can be used as geomorphic marker (e.g., Clementucci et al., 2023a; Marder et al., 2023; Moumeni et al., 2023). Indeed, in the  $\chi$ - $z$  plot, the slope of the transformed river profile is the  $k_{sn}$ , considering the integral quantity  $\chi$  as independent variable. In a region with minimal spatial variation in bedrock erodibility and precipitation, river steepness adjusts to the pattern of rock uplift. In this term, the integral approach represents an effective tool to identify and discretize the knickpoints (Perron & Royden, 2013; Royden & Taylor Perron, 2013). In particular, non-lithological knickpoints should cluster in a narrow range of  $\chi$  values (Perron & Royden, 2013) and separate stream segments with different  $k_{sn}$  values (slope patches; Clementucci et al., 2023a; Royden & Taylor Perron, 2013; Schildgen et al., 2012). Knickpoints associated with heterogeneities and lithological contrasts are expected not to migrate upwards (or very slowly), and thus not show a significant break in  $\chi$  space (Kirby & Whipple, 2012). Similarly, minor knickpoints usually show a small slope-break along the channels in  $\chi$ -space, without a significant variation of  $k_{sn}$  values. By using this approach, knickpoints were divided into three categories: non-lithological, minor, and lithological knickpoints (Table S2 in Supporting Information S1).

A detailed analysis of knickpoints was performed by examining the shape of river profiles in longitudinal and  $\chi$ - $z$  plots (*i.e.*, knickpoints that experienced a similar rock uplift history should cluster in the  $\chi$ - $z$  plot; Clementucci et al., 2023b; Moumeni et al., 2023), using available geological maps (1:100.000 and 1:50.000 geologic map of Italy; Brozzetti et al., 2017a; Ghisetti & Vezzani, 1983; Iannace et al., 2004; Servizio Geologico d'Italia, 1971) and satellite imagery on Google Earth. The fluvial network and channels were extracted and modeled using the MATLAB software TopoToolbox (Schwanghart & Scherler, 2014) and a series of MATLAB functions (TAK - Topographic Analysis Kit; Forte & Whipple, 2019).

### 3.4. River Projections

We quantified the magnitude of incision by reconstructing the river projection downstream of non-lithological, transient knickpoints, and subtracting the modeled river elevation at the mountain front from the modern profile elevation, assuming  $\theta_{ref} = 0.45$  (Table S3 in Supporting Information S1; e.g., Clementucci et al., 2023a; Schildgen et al., 2012). This approach allows estimating the paleo-base level and hence the magnitude of incision and/or surface uplift since the onset of knickpoint migration (Clementucci et al., 2023a; Heidarzadeh et al., 2017; Moumeni et al., 2023; Schildgen et al., 2012). The amount of long-term incision represents the minimum value of incision because long-term denudation and lowering of the uplifted low-relief landscape also occurred (although it is assumed to be negligible).

### 3.5. Rock-Uplift History

We performed river linear inversions of six rivers draining the Castrovillari basin and the Cozzo del Pellegrino Massif to estimate the rock-uplift rates over time. Under conditions of uniform erodibility ( $K$ ), assuming  $n = 1$ , a block uplift scenario, and no substantial changes in the drainage area over time (e.g., river capture), variations in  $k_{sn}$  values can be interpreted to reflect the fluvial response time to base level fall, following rock uplift variations (Goren et al., 2014). Specifically,  $\chi$  can be converted into time allowing to explore the timing of upstream propagation of transient knickpoints. Here, we used the MATLAB code provided by Goren et al. (2014) and Racano et al. (2023), where the integral version of the stream power of Equation 2 can be inverted to define the non-dimensional rock-uplift rate ( $U^*$ ). This corresponds to the slope of the  $\chi$ -plot and allows to infer the rock uplift history of the catchment (Clementucci et al., 2023b; Goren et al., 2014; Racano et al., 2023).  $\chi$  and  $U^*$  were

then converted to fluvial response time ( $\tau$ ) and rock-uplift rate ( $U$ ) by using estimates of rock erodibility for our study area (Goren et al., 2014):

$$U = KA_0^m U^* \quad (4)$$

$$\tau = \frac{\chi}{KA_0^m} \quad (5)$$

We selected basins characterized by similar bedrock erodibility, primarily limestone and metalimestones (Bonardi et al., 1988), and without any evidence of drainage area gain or loss. We tested two models by using  $m$  equal to 0.45, as used for the regional-scale fluvial analysis presented in this study, and 0.4 which represents a consistent value for Southern Apennines, as used in previous studies (Gallen et al., 2023; Olivetti et al., 2012). Similarly, the erodibility constant ( $K$ ) for each drainage basin was estimated using the stream-power law ( $K = E/k_{sn}^n$ ) and considering:  $n = 1$ , basin-averaged  $k_{sn}$  values for  $m = 0.45$  and  $0.4$  (Table S4 in Supporting Information S1), and for basin-average erosion rates ( $E$ ), the long-term uplift rate recorded by the stepped marine terraces along the Ionian side (Santoro et al., 2009). Specifically, we considered the oldest marine terrace (407 ka) which shows an averaged uplift rate of 1.2 mm/yr. This value is then divided by the mean value of the six basin-averaged  $k_{sn}$  as summarized in Table S4 in Supporting Information S1, to quantify the  $K$  value. The rock-uplift histories were then aggregated by computing mean and standard deviation values, providing a comprehensive representation of the overall trend in rock-uplift rates over time, following the same approach of Clementucci et al. (2023b). Finally, the rock-uplift history was critically assessed by comparing the linear inversion results with stratigraphical and geomorphological constraints.

## 4. Results

### 4.1. Structural Data

Here, we present our structural results including new cross-cutting slickenline populations, providing additional time constraints for the variations in the tectonic transport direction along the faults bordering the three main basins: (a) the Castrovillari, (b) the Campotense and (c) the Mercure (locations and data in Figure 2, Figure S2 and Table S1 in Supporting Information S1). The result will be compared with previous studies in the discussions.

1. The Castrovillari basin is bordered by the Pollino fault, which overall strikes NW-SE. On the southeastern tip of the Pollino flank (Sites 25–30; PF in Figure 2), we measured a local fault plane striking slightly  $\sim N280^\circ$ , with clear right-lateral kinematic indicators and highly oblique slickenlines suggesting a tectonic transport direction oriented  $\sim N140$  (Figure 4; Site 28). Similarly, further southeast facing the Sibari Plain, we measured a subvertical fault striking NW-SE with oblique slickenlines (Figure 4; Site 31). The Castrovillari basin is also characterized by a system of faults cutting through the infilling sediments, with fault scarps striking approximately  $N150^\circ$ . Kinematic analysis on these faults reveals a tectonic transport direction oriented  $\sim N220^\circ$  (Figure 2, Figure S2 and Table S1 in Supporting Information S1; Sites 21–24).
2. The Campotense basin is located further west than the Castrovillari basin (Figures 2 and 6a). It is bordered to the north by the western continuation of the Pollino fault, which strikes E-W at this location (PF in Figure 2). We measured fault planes striking  $\sim N100^\circ$  (Figures 2 and 4; Sites 8–15) with two slickenline populations with cross-cutting relationships changing from oblique- (Site 8) to dip- (Sites 11–13–14) slip, with tectonic transport directions oriented  $\sim N280^\circ$  and  $N160^\circ/N200^\circ$ , respectively. To the east, the Campotense basin is also bordered by a N-S-striking set of faults that apparently disconnect the Campotense basin from the Castrovillari basin. There, we measured fault planes striking  $\sim N-S$  (Figure 2; Sites 16–19, 33; Figure S2 in Supporting Information S1) with complex kinematics and a relative chronology indicating a swing from oblique- (Figure 2 and Figure S2 in Supporting Information S1; Sites 19–17; Figure 4; Site 17) to dip- (Figure 2; Sites 17–18–19) slip, in association with a tectonic transport directions oriented  $\sim N340^\circ$  and  $\sim N270^\circ$ , respectively.
3. The Mercure basin is the westernmost tectonic depocenter of the study area (Figure 2) bordered by a south-westward dipping fault. In the northwestern tip of the Mercure basin, we measured different fault planes lying at different elevations (Figure 2 and Figure S2 in Supporting Information S1; Sites 1, 2 and 3) and striking  $\sim N130^\circ$  with two different families of slickenlines, one oblique (Figure 4 and Figure S2 in Supporting Information S1; Sites 1, 2 and 3) and one dip-slip (Figure S2 in Supporting Information S1; Site 2), with



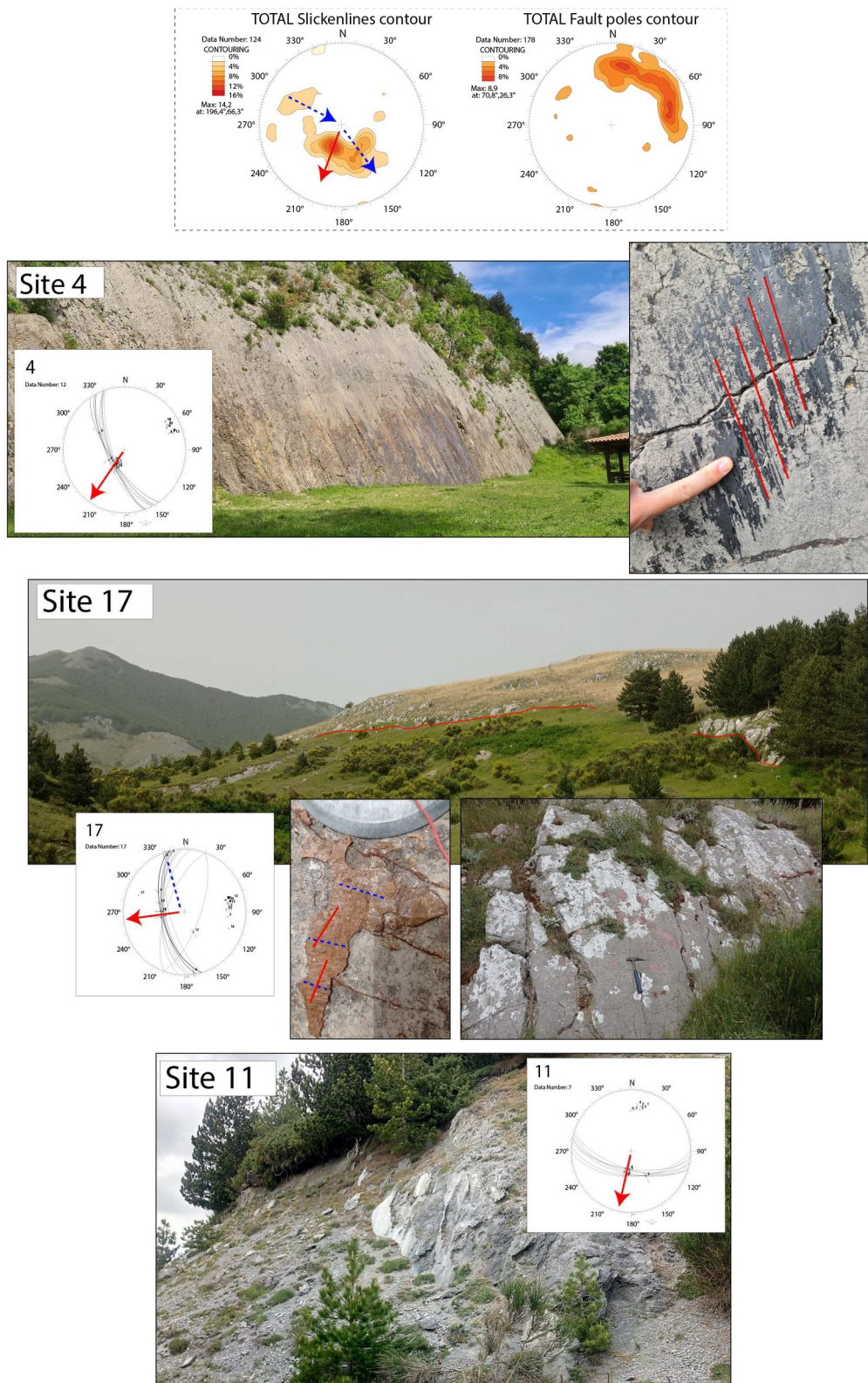


**Figure 4.** The upper part of the figure shows cumulative lower hemisphere Schmidt net of the slickenlines contour and fault poles contour merging all data collected in the field. The first tectonic transport direction, oriented ca N120°/150°, is shown with dashed blue arrows, while the most recent tectonics transport direction, oriented ca N200°, is shown with red arrow. Below, outcrop views for some stations of measurements (Stop 4, 17, 11, 28, 31, 1; see locations in Figure 2). For each structural stations, we show details of kinematic indicator and/or slickenlines together with the stereoplots. Details of all measurement are reported in the supporting information.

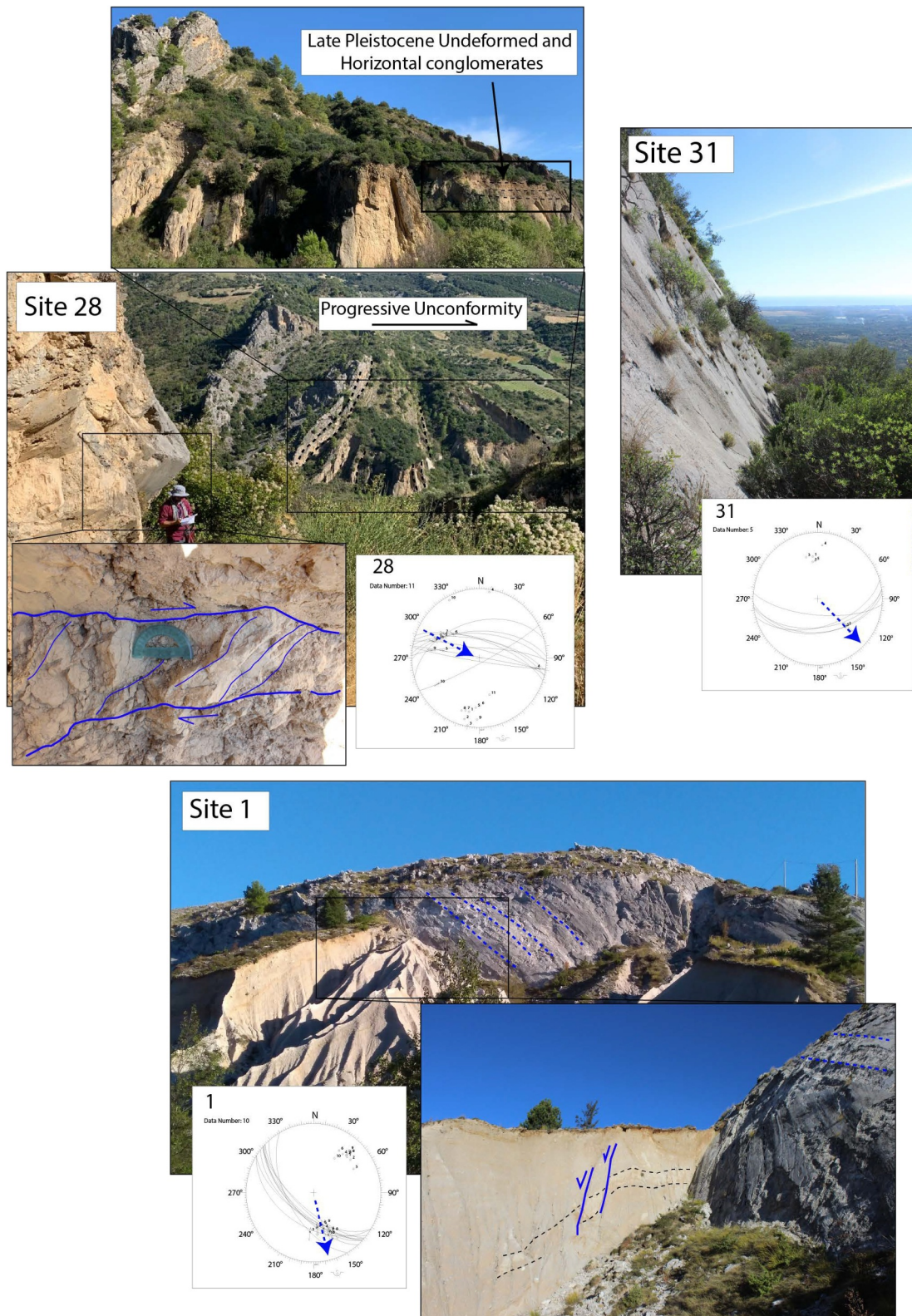
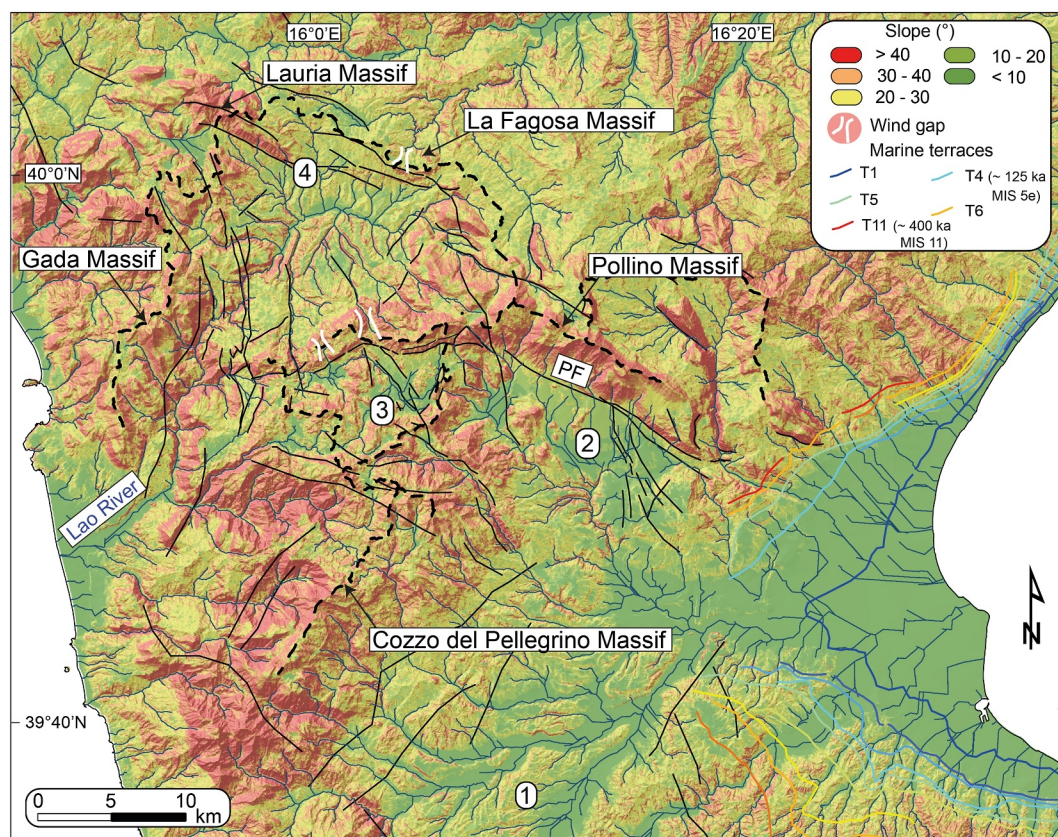


Figure 4. (Continued)



**Figure 5.** Slope map with Quaternary normal faults (black thin lines). Middle Pleistocene–Holocene marine terraces on the Ionian coast of northern Calabria are reported (after Cucci, 2004; Santoro et al., 2009). Dashed black lines are the main local drainage divide. (1) Crati basin; (2) Castrovillari basin; (3) Campotenese basin; (4) Mercure basin. PF: Pollino Fault.

tectonic transport directions oriented  $\sim N165^{\circ}/180^{\circ}$  and  $\sim N200^{\circ}$ , respectively (in agreement with previous observation provided by Brozzetti et al., 2009). Conversely, in the eastern Mercure basin we measured a well-exposed fault locally covered by hematite mineralization striking  $\sim N150^{\circ}$ , with overall dip-slip kinematics and a tectonic transport direction oriented  $\sim N225^{\circ}$ , toward the center of the basin (Figure 4 and Figure S2 in Supporting Information S1; Site 4). It is worth noting that this represents the first case of hematite fault in carbonate described in the Apennines suggesting a circulation of hot fluid.

#### 4.2. Regional Topographic Analysis

The Pollino Massif and surrounding mountains are characterized by high-relief, deeply incised morphology with steep flanks. The maximum topography is locally constituted by low-relief upland surfaces alternating with mountain peaks higher than 2,000 m (i.e., Pollino, Gada, Cozzo del Pellegrino and Lauria mountains; Figures 2 and 5; Figure S3 in Supporting Information S1). The intermontane basins at lower elevations ( $\sim 400$  and 1,000 m) are characterized by low-relief paleosurfaces and depositional surfaces locally dissected by deep valleys (i.e., Mercure, Campotenese and Castrovillari basins; Figures 2, 5 and 6; Figure S3 in Supporting Information S1). The highest peaks of the study area, range between 1,500 and 2,300 m in elevation and reach a maximum in the Pollino Massif (2,248 m). The main mountain ridges (Pollino, La Fagosa, Lauria, Gada and Cozzo del Pellegrino Massifs) show high values of slope and local relief, higher than  $40^{\circ}$  and 1,000 m, respectively, and are usually located in the hanging-wall of the Quaternary normal faults (Figure 5 and Figure S3 in Supporting Information S1). The average elevations of the Mercure, Campotenese and Castrovillari basins are 500, 1,000 and 400 m, respectively (Profile 1 in Figure 2). On the top of terrace surface and near the incised valleys the slope values range, respectively, between  $5^{\circ}$ – $10^{\circ}$  and  $30^{\circ}$ – $40^{\circ}$  (Figures 5, 6d and 6e).

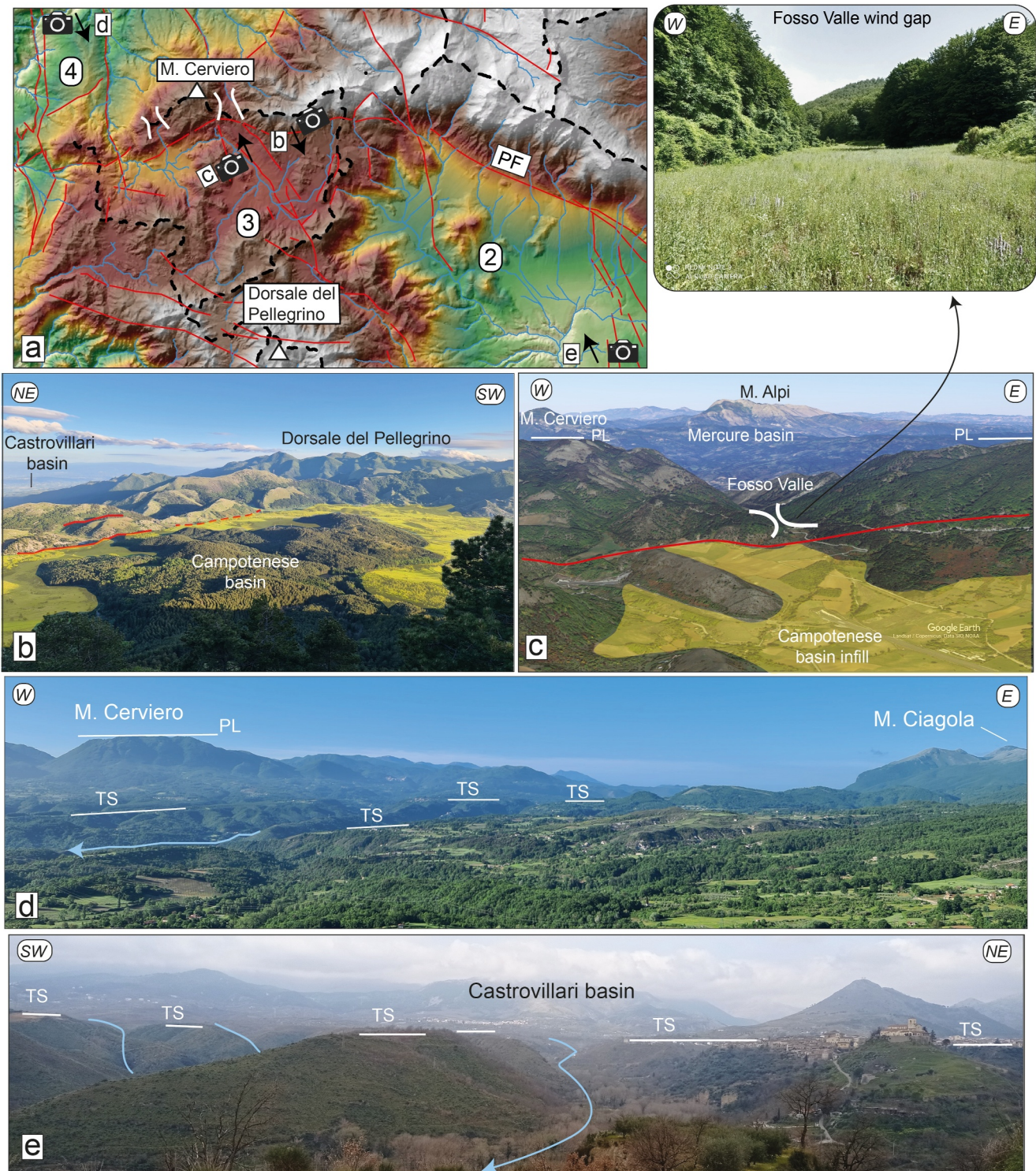


**Figure 6.** (a) Topographic map of the Campotenese basin delimited by the dashed white lines. (b, c) Pictures of the northern and southern boundary of the Campotenese basin (3), respectively. Note, the basin fill onlapping against the fault scarps. White lines denote the presence of wind gap. (d) Panoramic view of the Mercure basin from Castelluccio Superiore (4). (e) Panoramic view of the Castrovillari basin (2). Note, the abrupt transition from steep incised valleys and flat top depositional surfaces of the basin fill, now forming incised terraces. PL: Paleo-landscape. TS: Terrace surface. PF: Pollino Fault.

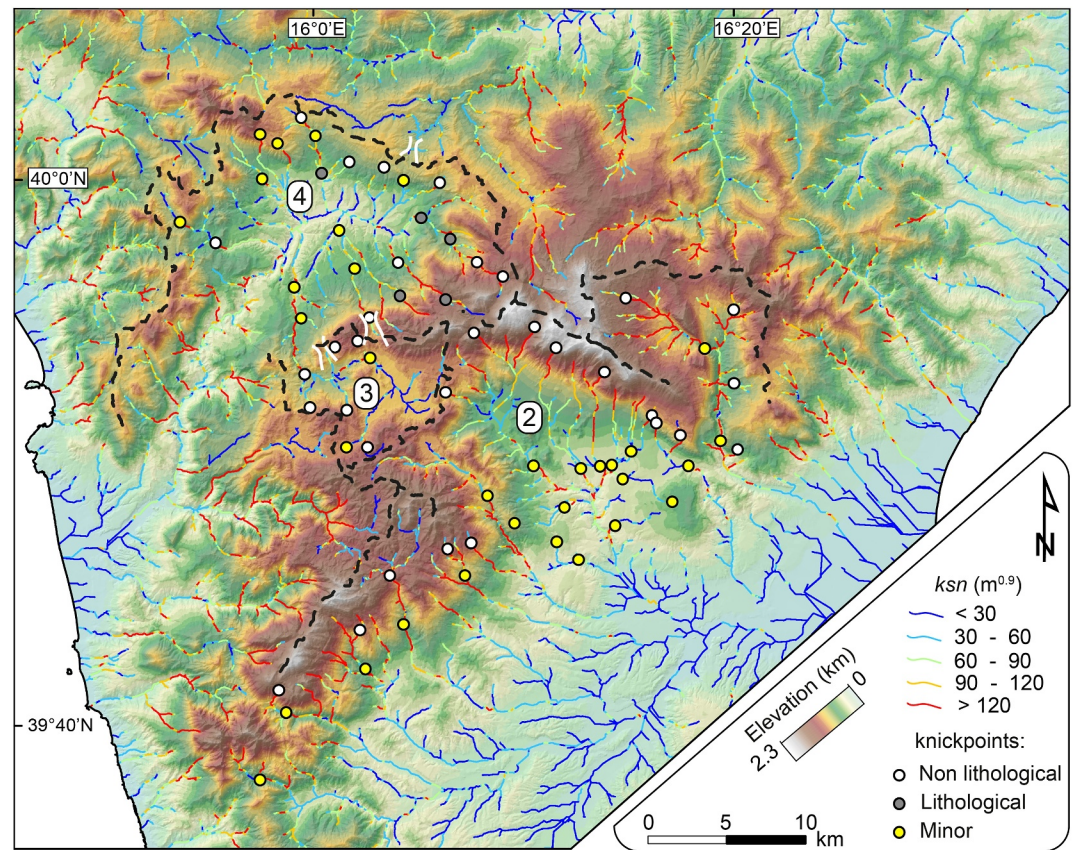


**Figure 7.**  $k_{sn}$  values with main knickpoints of the rivers draining the Castrovillari, Campotense and Mercure basins. Dashed black lines are the main local drainage divide. (2) Castrovillari basin; (3) Campotense basin; (4) Mercure basin.

The basin infill is mostly composed of Quaternary (at least until  $\sim 515$  ka in the Mercure; Robustelli et al., 2014) continental and marine-continental sedimentary sequences in the Mercure-Campotense and Castrovillari, respectively (Figures 6b and 6c; Chiarella et al., 2021; Robustelli et al., 2014). The flat topography within these basins marks the top depositional surface (Chiarella et al., 2021; Schiattarella et al., 2003). Along the Ionian coast and inland in the Sibari plain, well-preserved flights of late Quaternary marine terraces show up to eleven orders of terraces (Lucà et al., 2022; Santoro et al., 2009). Several wind gaps were recognized on the main local drainage divide along the N and NE borders of the Campotense and Mercure basins (Figures 6a and 6c).

### 4.3. River Morphology

We examined the river networks of the Mercure, Campotense and Castrovillari basins (basin 2, 3 and 4 in Figure 5), whose water divide is near the Pollino mountain range (dashed black lines in Figure 5). Specifically, we analyzed the regional  $k_{sn}$  patterns and longitudinal profiles of 47 main river segments (Figures 7 and 8 and Table S2 in Supporting Information S1), with 25, 8 and 14 rivers draining the Castrovillari, Campotense and Mercure basins, respectively.

The regional  $k_{sn}$  pattern shows locally low values of  $k_{sn}$  (0 and  $60 \text{ m}^{0.9}$ ) at the maximum topography, upstream of the non-lithological knickpoints with a general increase  $k_{sn}$  moving downstream toward the basin fill (Figure 7). The  $k_{sn}$  of the streams in the intermontane basins show an overall decrease downstream toward the coastal plain. Downstream of the minor knickpoints, at the transition between the basin fill and the coastal plain,  $k_{sn}$  locally increases (Figure 7). The Castrovillari and Cozzo del Pellegrino rivers drain toward the Ionian Sea, with a NW–SE flow direction (basin 2 in Figures 2 and 5). Longitudinal river profiles have an overall concave-up shape and are characterized by minor knickpoints between 200 and 800 m, and major non-lithological knickpoints with a mean elevation of  $1,117 \pm 75$  m (Figure 7 and Table S2 in Supporting Information S1). Minor and non-lithological knickpoints cluster approximately at values of  $\chi$  of 5–15 and 12–16, respectively (Figure 7b). The

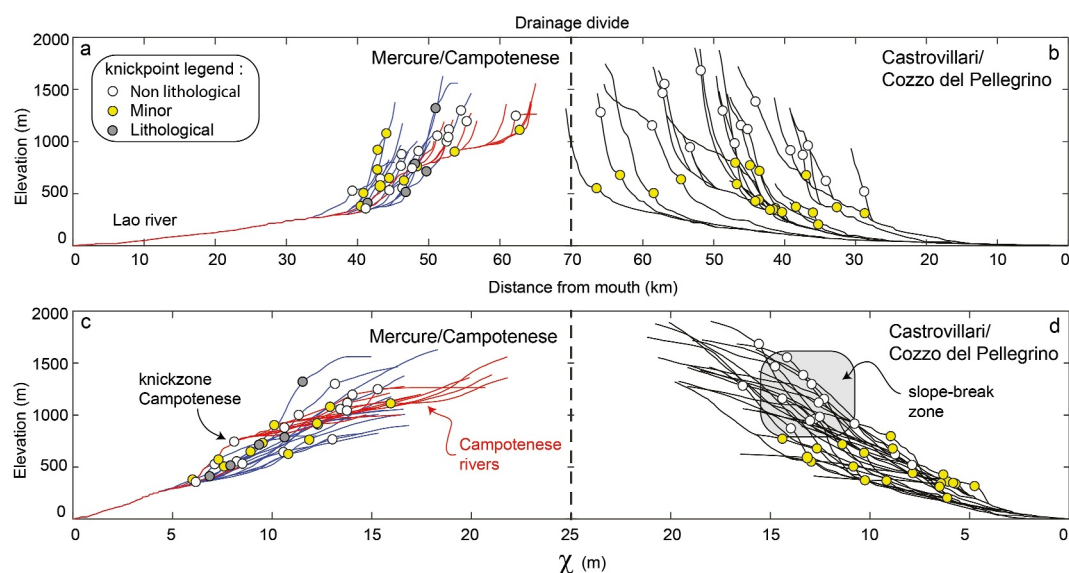


**Figure 8.** Longitudinal river profiles (a, b) and  $\chi$ -z plot (c, d) with knickpoints for the Castrovillari-Cozzo del Pellegrino (black rivers; basin 2 in Figure 5), Campotense (red rivers; basin 3 in Figure 5) and Mercure (blue rivers; basin 4 in Figure 5) basins. The non-lithological knickpoints are located at the slope-break zone separating segments with different  $k_{sn}$  values.

rivers' longitudinal and  $\chi$  profiles are steep downstream of non-lithological knickpoints, and gentle and rectilinear upstream (slope-break zone; Figures 7b and 7d). In particular, minor knickpoints are mainly lying above the terrace surface associated with the basin infill (Figure 6e).

The Campotense basin is a tributary of the Mercure basin, and its rivers exhibit transient longitudinal profiles. A wide knickzone is located at  $\sim 800$  m elevation. Non-lithological knickpoints lie between 1,000 and 1,250 m, yielding an average of  $1,000 \pm 133$  m, while minor knickpoints are found between 750 and 1,110 m (Figures 7a and 7c; Table S2 in Supporting Information S1).

The Mercure rivers drain the Lauria, La Fagosa and Gada and the basin is characterized by a complex drainage network, flowing toward the NW and sharply turning with a SW-directed flow into the Lao gorge (Figure 2). Rivers show concave-up and transient longitudinal profiles and contain minor and lithological knickpoints distributed across a wide range of elevations (Figures 7a and 7c), while non-lithological knickpoints are localized between 500 and 1,000 m, yielding an average of  $756 \pm 57$  m a.s.l. (Figure 7 and Table S2 in Supporting Information S1).

Generally, non-lithological knickpoints of the study area are found at an average elevation of  $960 \pm 100$  m and mark a sharp variation in  $k_{sn}$  values (Figure 8; Table S2 in Supporting Information S1). Conversely, we do not observe significant variation in channel slope upstream and downstream of minor knickpoints, except for a local slope break in the longitudinal profile (Figures 7 and 8).

#### 4.4. Magnitude of Long-Term Incision

To estimate the long-term fluvial incision, we selected the highest non-lithological knickpoints described above, which lie mainly above the carbonate bedrock (Figure 8).

The Castrovillari and Mercure-Campotense river systems (here considered together as the same river system) flow directly into the Ionian and Thyrrenian Seas, respectively. For the Campotense and the Mercure basins, the presence of wind gaps and sharp variations in the drainage pattern indicates a recent dynamic reorganization that is likely tectonically controlled (Filice & Seeber, 2019). Conversely, the lack of such evidence in the Castrovillari basin suggests that the Ionian Sea remained the base level of the Castrovillari river system at least since the last base level fall (*i.e.*, the one associated with the opening of the basin and the establishment of the current exorheic conditions). Furthermore, the overall progradation direction of the Gilbert-deltas points toward the Ionian Sea, suggesting the existence of reliefs in the Pollino and Campotense area and a flow direction similar to the modern

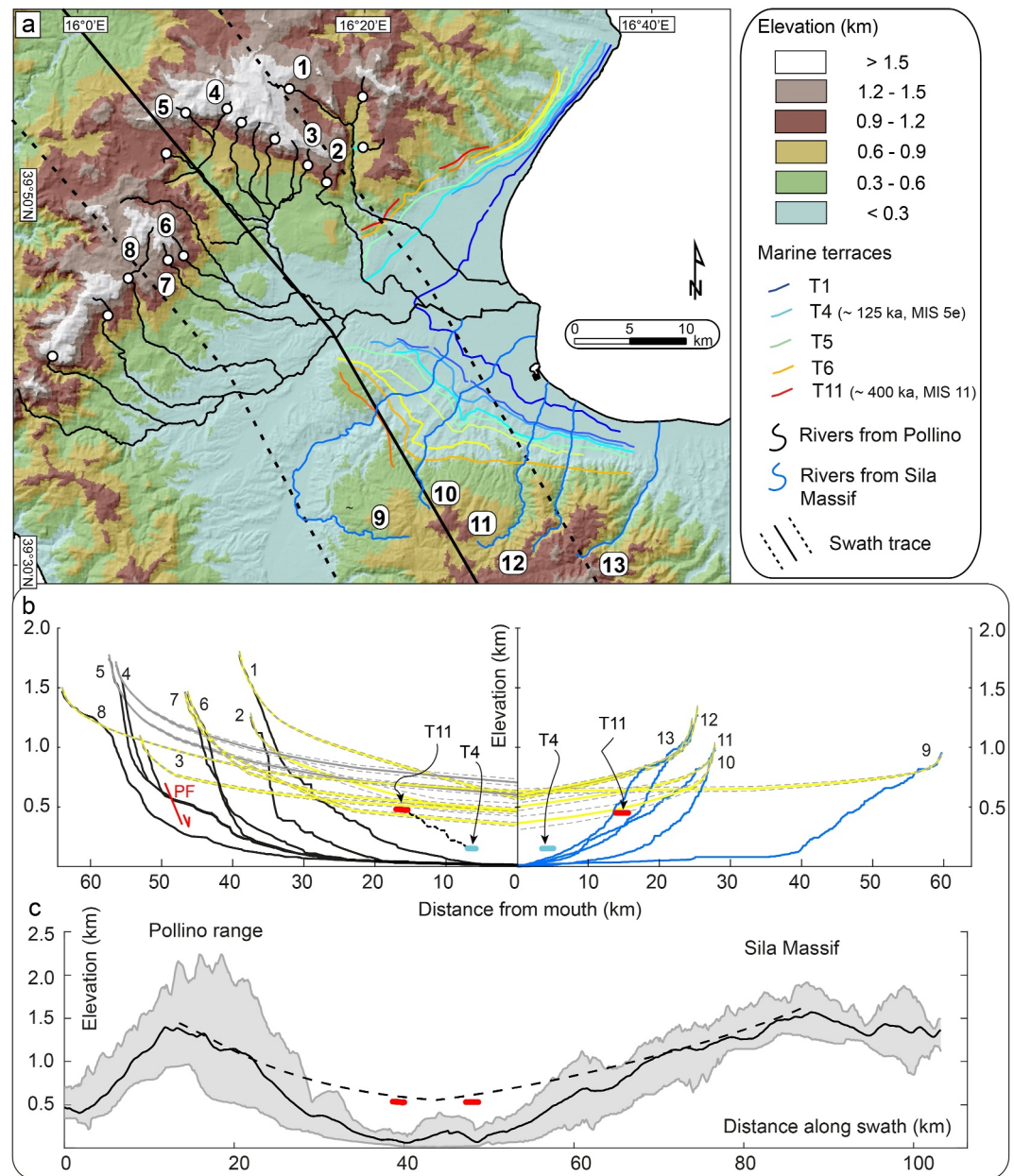


**Figure 9.** (a) Topographic map of the Pollino and Sila Massif. (b) Modern longitudinal profiles and projections of the relict landscape (red segments) upstream of the highest knickpoints using  $\theta_{ref} = 0.45$  and the  $k_{sn}$  of the relict portion of selected rivers (bold rivers in panel a). The main values of long-term fluvial incision are at  $\sim 500$  m for both Pollino-Cozzo del Pellegrino and Sila range (see details in Table S2 in Supporting Information S1). Gray river projections are two rivers flowing Castrovillari basin (see main text for details). Reported marine terraces from T11 to T1 reflect the oldest and the youngest, respectively (Santoro et al., 2009). (c) Swath profile (details and location are shown in panel a) with data from river projections and uplifted terraces from Santoro et al. (2009) and Olivetti et al. (2012). PF: Pollino Fault.

one (Chiarella et al., 2021; Colella, 1988; Colella et al., 1987). We therefore calculated the magnitude of fluvial incision by reconstructing the paleo-channel profiles from the rivers flowing through the Castrovillari basin and Cozzo del Pellegrino Massif (knickpoints in the slope-break zone in Figure 8d). Estimated values of fluvial incision for these rivers based on 8 stream profiles range from 340 to 700 m, with an average of  $527 \pm 40$  m (Figure 9 and Table S3 in Supporting Information S1). Rivers 4 and 5 drain the highest peaks of the Pollino range and show the highest incision values in the study area (gray projection in Figure 9b). For comparison, we calculated fluvial incision on the northern margin of the Sila Massif, which should have experienced a similar

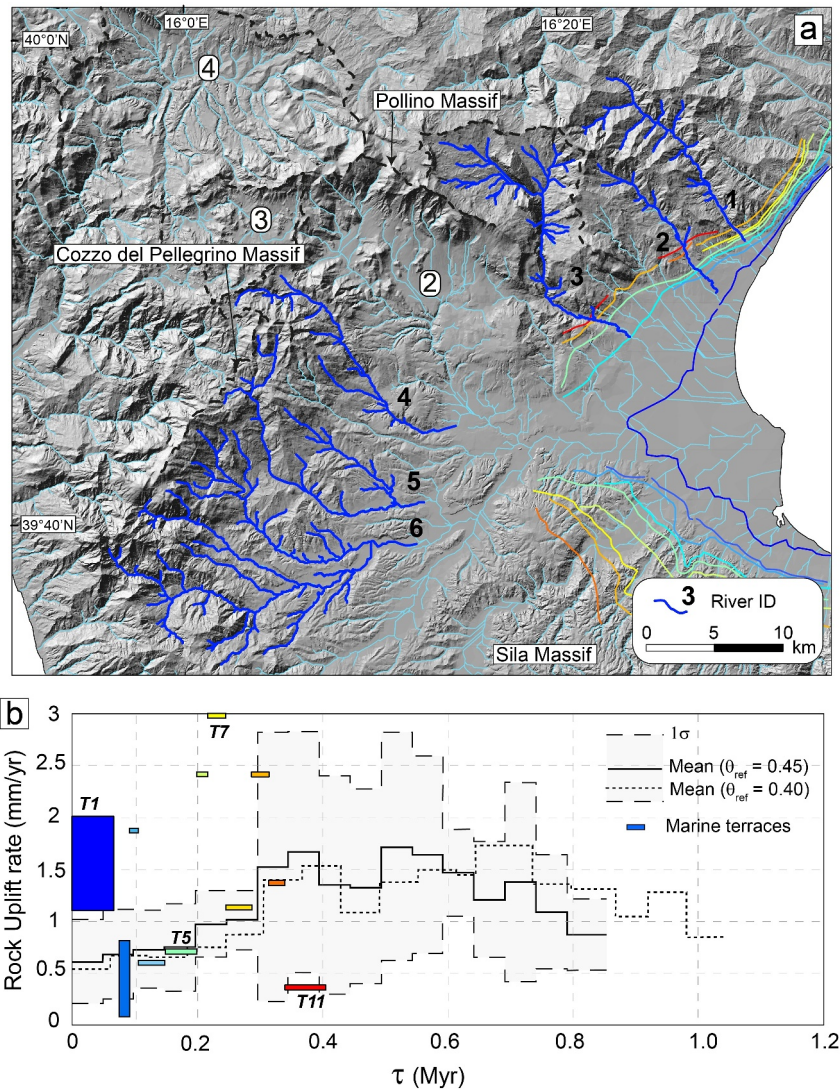


**Figure 10.** (a) Hillshaded model with rivers selected for the linear inversion draining the Pollino and Cozzo del Pellegrino Massif (River ID data are provided in Table S4 in Supporting Information S1). (b) Response time versus mean rock-uplift rates and associated standard deviation values for two different concavity values, along with uplift rates from marine terraces in the Pollino area (data of central sector from Santoro et al., 2009). Note the rock-uplift history using a reference concavity ( $\theta_{ref}$ ) of 0.45 results slightly younger than 0.40. The colors of marine terraces reflect the order as mapped by Santoro et al. (2009).

temporal topographic evolution. There, the magnitude of fluvial incision calculated by projecting 5 rivers is between 360 and 600 m, with an average of  $526 \pm 45$  m (Figure 9 and Table S3 in Supporting Information S1). Overall, our estimates of long-term river incision for the Pollino Massif are on the same order as those for the Sila Massif. The topographic relief predating the long-term base level fall in the Pollino and surrounding ranges was estimated by calculating the difference between the modern mean drainage divide elevation and the elevation of the outlet of the reconstructed river profiles. We obtained maximum estimates of topographic peaks of  $\sim 1,700$  m and  $\sim 1,300$  m for the Pollino and Sila Massifs, respectively (Figures 9b and 9c).

#### 4.5. Rock-Uplift History

Our river inversion analysis has been performed by using  $n = 1$ ,  $m/n = 0.45$ , and an erodibility  $K$  of  $12.8 \times 10^{-6} \text{ m}^{0.1}/\text{yr}$ . We then compared these results with river inversion using  $m/n = 0.4$  and  $K$  of  $28.2 \times 10^{-6} \text{ m}^{0.2}/\text{yr}$  (Figure 10b). The estimates of  $K$  values are consistent with those observed in other



tectonically active regions (Stock & Montgomery, 1999) and higher than quiescent tectonic settings (Clementucci et al., 2022). Interestingly, they are slightly higher but in the same order of magnitude of estimates from the Northern Apennines and NE Sicily, respectively, where carbonate lithologies are also exposed (Fisher et al., 2022; Pavano & Gallen, 2021). All the selected rivers show a similar rock-uplift history and  $U^*$  (non-dimensionalized rock-uplift rate) starting approximately from 800 ka, despite few minor knickpoints, which cause spikes in the overall uplift trend (Figure S4 in Supporting Information S1). The highest mean uplift rates are reached between 600 and 300 ka and range from 1 to 1.7 mm/yr despite the large variability (i.e., high standard deviation; Figure 10b), which is due to localized variations in the  $\chi$  profile of the different rivers (Figure S4 in Supporting Information S1). From 300 ka to present-day, the rock-uplift rates decrease gradually with a mean value of 0.5 mm/yr, and a lower standard deviations (Figure 10b). The trend of rock-uplift modeled by normalizing  $k_{sn}$  with reference concavity of 0.4 and using  $K = 28.2 \times 10^{-6} \text{ m}^{0.2}/\text{yr}$ , show a similar spatial pattern with a slightly older history, starting from 1 Ma (Figure 10b). Overall, the modeled rock-uplift rates are consistent with the uplift rates obtained from marine terraces for the 400 to 100 ka time intervals. From 100 ka, however, the inferred rock-uplift rates do not match with those estimated from marine terraces (Figure 10b).

## 5. Discussion

### 5.1. Fault System: Kinematic Analysis and Timing of Deformation

Numerous studies have reported fault slip directions along various portions of the investigated area (see a recent database published by Lavecchia et al., 2024), describing contrasting scenarios for the evolution of the Southern Apennines. For example, Papanikolaou and Roberts (2007) averaged all the slip directions, merging different slickenlines populations. They interpreted their oblique-slip direction as related to the shear stress generated at the fault tips, and concluded that only extension was active in the region. In contrast, along the Mercure basin, Brozzetti et al. (2009) documented a swing in the tectonic transport direction from left-lateral to dip-slip suggesting that the opening of the basin was related to extensional activity. This observation contradicts the one proposed by Filice and Seeber (2019), who suggested a transition from thrust to normal kinematics caused by a tectonic collapse, leading to the opening of the Mercure basin. Moving southward, in the Pollino Range, Ferranti et al. (2009) documented another complex scenario invoking a NE-SW direction of shortening, controlling the left-lateral kinematics, along with a broad N-S direction of shortening, active up to 215 Kyr, as suggested by folds measured within conglomerates.

Our cumulative structural analysis reveals two equal peaks of fault populations, primarily striking north-south and east-west, dipping westward and southward, respectively (fault poles contour in Figure 4). Moreover, the tectonic transport directions show a major peak at N210° (slickenlines contour in Figure 4) and a second minor tectonic direction at ca. N120°/150° (slickenlines contour in Figure 4). Slickenlines cross-cutting relations suggest a swing in the tectonic transport direction, changing from N120°/150° with a left-lateral component to N210° with a dip-slip kinematics. Thus, the overall picture provided by our work is consistent with the findings of Brozzetti et al. (2009, 2017a). However, the temporal relationship between these two tectonic transport directions remains unclear and can only be inferred through independent stratigraphic constraints. An example is the right-lateral fault striking E-W (Figure 2; Sites 28–30), which is sealed by late Pleistocene undeformed and horizontal conglomerates (Figure 4, see also Chiarella et al., 2021; Ferranti et al., 2009). We interpret this E-W fault strand as the conjugate of the overall left-lateral deformation system occurring along NNW-SSE fault strands, associated with the N120°/150° tectonic transport (e.g., Brozzetti et al., 2017a; Ferranti et al., 2009). Consequently, the timing of the end of the initial tectonic regime (the one oriented N120°/150°) remains uncertain but likely occurred during the middle Pleistocene. On the contrary, the second tectonic transport direction, oriented N210°, is likely more recent, as it has been measured on faults with a clear morphological expression, such as the N-S faults within the Castrovillari basin (Figure S2 in Supporting Information S1; Sites 21–24). Furthermore, this later tectonic regime is still active, as deduced by seismological trenches and recent earthquake focal mechanisms (Brozzetti et al., 2009, 2017a; Cinti et al., 1997, 2002; Michetti et al., 1997).

In summary, the kinematic change from left-lateral to dip-slip documented here, aligns with findings reported by some of the previous authors (e.g., Brozzetti et al., 2009, 2017a). Interestingly, while the left lateral motion along the Southern Apennines has been linked to the rollback migration of the Calabria arc (e.g., Hippolyte et al., 1994; Monaco et al., 1998; Scandone, 1979; Schiattarella, 1998; Schiattarella et al., 1994), the origin of the N210° dip-slip kinematic that led to the opening the intermontane basins, can be explained by both backarc extension and/or

extensional collapse due to a gradient in potential energy acquired during regional uplift (D'Agostino et al., 2014).

## 5.2. Drainage System: Fluvial Evolution and Correlation With Geomorphic Markers

The fluvial network and the examples of headwater captures, testified by observed wind gaps, record a tectonic control on the morphological evolution of the study area (Figures 6–8; Robustelli et al., 2014; Willett et al., 2014). The rivers show two main groups of transient knickpoints indicating two possible phases of base level fall (Figures 7 and 8). The higher non-lithological knickpoints recorded the regional increase in the uplift rates (cumulative amount of ~500 m; Figure 9 and Table S3 in Supporting Information S1), as indicated by a clear slope-break zone and their clustering in a narrow range of  $\chi$ -values. They can be considered as the minimum magnitude of rock uplift over at least ~400 ka, since they approximately correlate downstream with the MIS 11 oldest terrace (407 Kyr; Santoro et al., 2009; Figure 9c). On the other hand, the modeled rock uplift rates generally increase from ~800 ka (Figure 10). These geomorphic markers allow us to better refine the timing for the onset of uplift between 400 and 800 ka. Interestingly, some of the rock-uplift rates inferred from inversions are consistent with the uplift rates obtained from marine terraces, indicating a good correlation with independent geological constraints (Figure 10b). However, the rates did not match on the last 100 ka, where uplift rates are well-constrained by the dated MIS 5e terrace (Figure 10b). This discrepancy in the youngest rates of uplift between rivers and marine terraces may reflect the lag time between an external perturbation on the river profile and the onset of terrace cutting (e.g., Tofelde et al., 2019; Vandenberghe, 1995). In our study area, rates of uplift and basin-wide denudation are very high (~900 m/Myr for the adjusted channel downstream of knickpoints; Olivetti et al., 2012) and channels may exceed the hillslope threshold, indicating a nonlinear relationship between  $k_{sn}$  and basin-wide denudation rates (e.g., Ouimet et al., 2009). Therefore, considering  $n > 1$ , our history of base level fall may be contracted and/or dilatated due to faster migration upstream of steeper slope patches compared to flatter ones, resulting in the loss of information into consuming knickpoints. This, in turn, can lead to a distorted inferred uplift history when using  $n \neq 1$  (Royden & Taylor Perron, 2013). Ultimately, our history of rock uplift represents a plausible scenario, considering  $n = 1$ , providing a time boundary for the onset of topographic rejuvenation in the Pollino and Sila regions (400–800 ka). A series of minor knickpoints lie at lower elevations, mostly on the top of terrace surfaces of the intermontane basins' infill deposits (Figure 6e). The break-point separates the deeply incised valleys from the terrace surfaces, suggesting their migration following base level lowering after the endorheic-exorheic transition (e.g., Struth et al., 2019). The drainage connection to the sea of the intermontane basins is considered the youngest geological event, even if it might not have occurred coevally from north to south (see the compilation of lacustrine deposits in Lanari, Reitano, et al., 2023). For instance, the external drainage connection of the Mercure Basin is younger than ~500 Kyr (Robustelli et al., 2014), but it is reasonable to infer that it occurred earlier than the external connection of the Castrovillari Basin, whose basin infill hasn't been fully incised yet. Conversely, the timing of the internal/external drainage evolution of the Campotense Basin is difficult to determine due to a lack of age constraints.

Locally, the drainage divides present high-standing wind gaps, usually located in the footwall of the Plio-Pleistocene major normal faults, as evidence of recent change in flow orientations and drainage capture (e.g., in Mercure basin from NE to SW). These features indicate the transition from internal drainage conditions, likely due to fault activity, to the re-opening of the basins toward the sea following new pathways (e.g., Lanari et al., 2021). The deep gorge of the Lao river is a clear example of incision promoted by the Mercure drainage connection with the Tyrrhenian Sea (Robustelli et al., 2014).

In summary, our fluvial and geomorphic analysis reveals strong evidence of drainage re-organization and phases of base level fall (*i.e.*, two distinct patterns of knickpoints) and allows us to reconstruct the main steps of the topographic evolution of the Southern Apennines.

## 5.3. Evolving Topography of Pollino Range and Surrounding Intermontane Basins

The Southern Apennines represent a complex region, where processes act at different spatial (from crust to mantle) and temporal scales (from Kyr to Myr; Ferranti et al., 2006; Cuffaro et al., 2011; Faccenna et al., 2011) and where markers of the last interglacial sea-level indicate a fast uplifting arc (Antonioli et al., 2006; Brozzetti et al., 2017a; Ferranti et al., 2006; Santoro et al., 2009). Structural and geomorphic markers such as knickpoints, high-standing marine and fluvial terraces, uplifted relict landscapes and river networks record the cumulative

vertical movements at least over the last few million years (Cucci, 2004; Meschis et al., 2022; Pavano & Gallen, 2021), offering the possibility to explore the magnitude and timing of the recent topographic rejuvenation and its relationship with the tectonic activity. By comparing our findings with published geological and geomorphological data, we propose possible stages for the structural and topographic evolution of the study area, as summarized in Figure 11. We discuss hereafter the processes acting at different scales: (a) the Pollino Massif and surrounding basins (<50 km); (b) the Southern Apennines and the Calabrian arc (>100 km; Sila and Pollino Massifs).

*Stage a:* The Southern Apennines wedge was partially uplifted, and therefore eroded and exhumed since the late Miocene due to orogenic accretion related to the subduction of the Adria-Ionian plate. This is well attested also by low-temperature thermochronology data and syn-sedimentary deposits (Lanari, Boutoux, et al., 2023; Lanari, Reitano, et al., 2023 and references therein Corrado et al., 2005; Invernizzi et al., 2008; Mazzoli et al., 2008; Vignaroli et al., 2012; Olivetti et al., 2017). Subsequently, the uplifted range was progressively eroded, promoting the development of low-relief topography, which may be diachronous from the inner to the outer portion of the chain (Amato & Cinque, 1999; Ascione & Cinque, 1999; Olivetti et al., 2017). The maximum topography of ~1,700 and ~1,300 m for the Pollino and Sila Massifs, respectively, can be interpreted as the paleo-relief, similar to that observed in the northernmost mountains of the Southern Apennines (Mt. Maddalena, Mr. Marzano; Ascione & Cinque, 1999; Schiattarella et al., 2017). At this stage, the southeastward drift of the Calabria subduction zone favored extensive left-lateral kinematics along NW-SE faults, as documented in the present and previous studies (Brozzetti et al., 2017a; Catalano et al., 1993; Cinque et al., 1993; Ferranti et al., 2009; Knott & Turco, 1991; Scandone, 1979; Schiattarella, 1998).

At the same time, the Castrovallari and Crati basins were dominated by the sedimentation of marine Gilbert-type deltas (Chiarella et al., 2021; Colella, 1988). Conversely, the current shape of the Mercure and Campotense basins suggests that they were originally connected to the east, toward the foreland (Filice & Seeber, 2019).

*Stage b:* Since 800–500 ka, a regional increase in uplift rates and a major phase of extensional deformation occurred in the Southern Apennines (Patacca & Scandone, 2007; Santoro et al., 2009; Tropeano et al., 2002). Additional evidence of regional uplift during this stage includes shallowing of marine deposits and uplift of the wedge-top basins in the Bradanic Trough (e.g., Sant’Arcangelo basin) and marine Gilbert-type delta systems deposited in the Castrovallari and Crati basins, and migration upstream of non-lithological knickpoints (Ascione et al., 2012; Chiarella et al., 2021; Colella, 1988; Spina et al., 2011; Tropeano et al., 2002). Interestingly, knickpoints and projections from the Pollino range (rivers 4 and 5 in Figure 9b) show a higher value of surface uplift, on the order of 600–700 m, indicating that they may result from the superimposition of regional (~500 m) and local footwall (100–200 m) uplift.

This uplift may have occurred during a changeover from left-lateral to normal faulting, likely coeval with the switch in kinematics observed along the northern and eastern border faults of the Campotense basin (see Figure S2 in Supporting Information S1; Site 8 and Figure 4; Site 17). The new prevailing normal faulting (see Figure 4) produced the fragmentation of Pollino and surrounding ridges, favoring the development of extensional, internally drained basins (Figure 11b; Brozzetti et al., 2017a; Russo & Schiattarella, 1992). The Mercure basin, and likely Campotense and Castrovallari basins, started to develop a structural depression accommodating the deposition of a succession of clastic sedimentary and lacustrine deposits (Robustelli et al., 2014; Spina et al., 2011). The well-documented infill of the Mercure basin consists of thinly bedded marly clays, reflecting a low-energy depositional setting such as a lacustrine system (Robustelli et al., 2014). The upper and lower age limits of the Mercure basin infill are 700 and 500 ka. These ages are constrained by a tephra within the lacustrine sediments ( $514 \pm 16$  ka) and the correlation with the well dated sediments of the nearby Sant’Arcangelo basin (~700 ka; Robustelli et al., 2014 and references therein).

*Stage c:* Between 500 and 400 ka, the Mercure basin may have experienced a base level fall, with the opening of the drainage toward the Tyrrhenian Sea through the development of the deep gorge of the Lao river, likely due to the headward erosion of knickpoints following the regional increase in uplift rates (Robustelli et al., 2014).

*Stage d and e:* From the late Pleistocene (<400 ka) to the present, the base level change recorded in the Campotense and Castrovallari basins marks a transition from endorheic to exorheic conditions (Figure 11d). The deep incision of the basin fill deposits is the result of headward erosion of the external drainage systems or lake overspill processes (Geurts et al., 2020; Heidarzadeh et al., 2017; Lanari et al., 2021). The upstream propagation

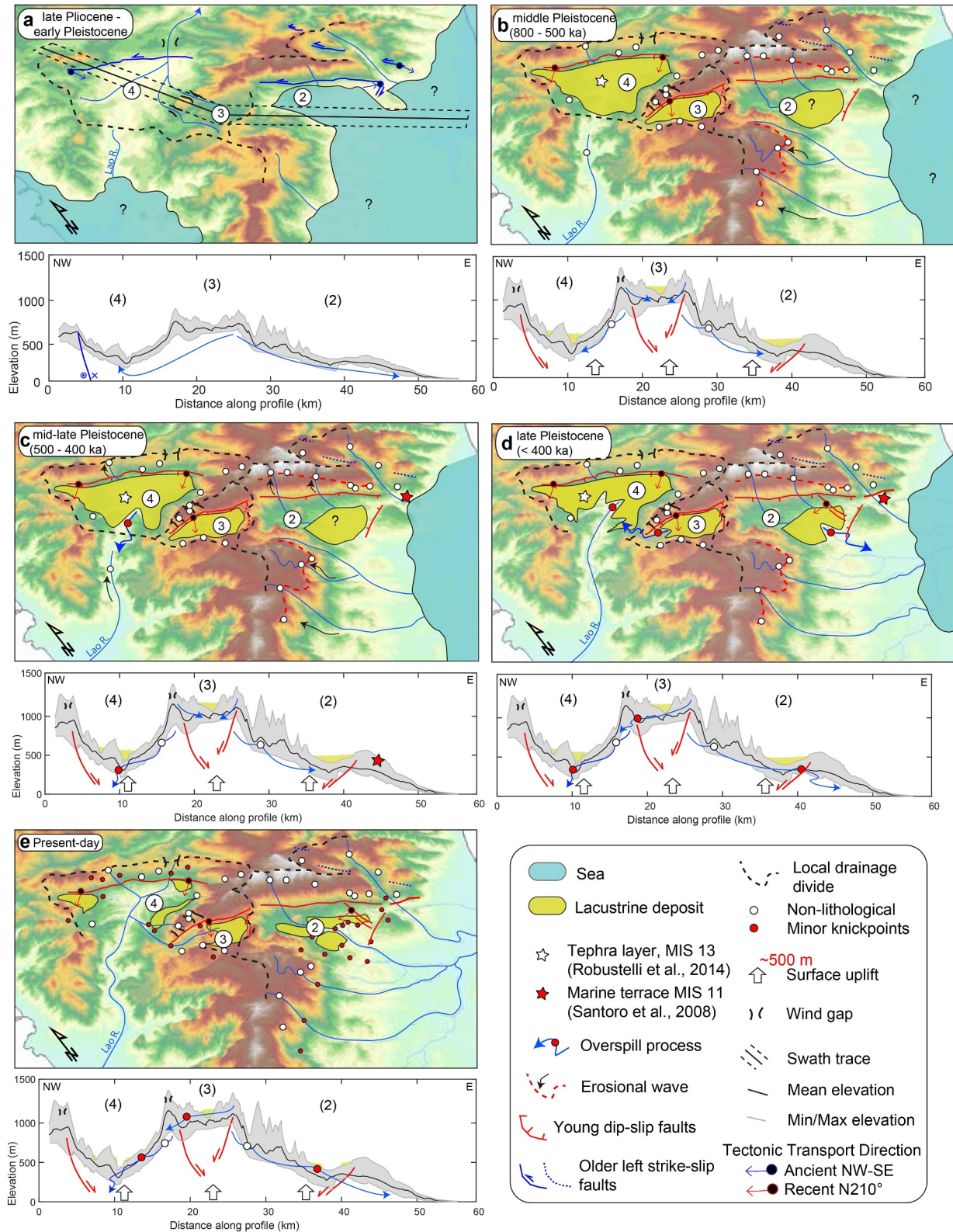


Figure 11.

of headward erosion through migration of minor knickpoints within the Castrovillari basin caused deep incision of the basin infill, creating strong disequilibrium conditions of the river network (Figures 11d and 11e). In the high-elevation Campotenese basin, the presence of wind gaps and a deep valley crossing the local divide may indicate river deflection toward the west into the Mercure basin following the progressive growth of Mt. Cerviero (*i.e.*, river lateral migration; Figures 6a, 10d and 10e). However, the Campotenese basin is presently connected to the Mercure basin by a wide knickzone and the alluvial deposits are still poorly incised, suggesting that the erosional wave caused by the recent base level fall has not yet fully propagated upstream. Simultaneously, the Mercure basin experienced the upstream propagation of the minor knickpoints to its present-day position in the range foothill, leading to significant incision of the basin infills.

#### 5.4. Uplift History and Mechanisms

The Southern Apennines result from the interplay between shallow and deep mechanisms. Within such domains, the narrow arcuate Calabrian Arc subduction zone, which presently migrates southeastward at a rate of 2–3 mm/yr (Palano et al., 2017), plays a critical role. Several phases of deformation occurred since the Miocene (*e.g.*, Mattei et al., 1999, 2007; Rossetti et al., 2001). In particular, two main deformation phases have been proposed for the Southern Apennines and Sicily since the late Miocene.

##### 5.4.1. Phase 1

The first tectonic phase results from the progressive rollback of the slab toward the SE, which produced compressional deformation and uplift at the front of the accretionary wedge during the early phase of subduction. The retrograde motion of the slab toward SE is attested in the Southern Apennines by the southeastward migration and rejuvenation of the foredeep deposits from Ariano to Sant’Arcangelo basins (Ascione et al., 2012; Patacca & Scandone, 2007; Tropeano et al., 2002). During this phase, counter-clockwise rotation of the Southern Apennines block and clockwise rotation of Sicily and Calabria is documented by paleomagnetic (Mattei et al., 2007) and geodetic data (Palano et al., 2017).

##### 5.4.2. Phase 2

The compressional phase is progressively substituted by long wavelength uplift and extension (Ascione et al., 2012; Filice & Seeber, 2019; Schiattarella et al., 2017; Tropeano et al., 2002). In the Southern Apennines, the second uplift phase is marked by the emergence of the Bradanic Trough, the previously formed wedge-top basins and marine Gilbert-type deltas, with topographic wavelengths over 100 km (Ascione et al., 2012; Colella, 1988; Tropeano et al., 2002). Similar kinematics and long wavelength signals have been suggested by Pavano and Gallen (2021) in northern Sicily: here, rock uplift histories derived from stream profiles suggest SE-directed migration of the Ionian slab (first peak of uplift due to crustal thickening), followed by a second peak of uplift related to the eastward migration of a slab window.

The recent long wavelength signal describes a progressive uplift decreasing from north to south, as highlighted by the elevation of MIS 5e marine terraces along the Ionian coast from 125 m in the Pollino area to 80 m in the Le Serre Massif (Faccenna et al., 2011; Nalin et al., 2020), and by <sup>10</sup>Be-derived denudation rates and uplifted erosional surfaces (Olivetti et al., 2012; Roda-Boluda et al., 2019; Figure 11b). These inferences, however, need to be confirmed, as the attribution of the terrace lying at 80 m to the MIS 5e highstand at Le Serre Massif is based on a cross-correlation basis, and no absolute ages exist (Figure 12b; Cucci, 2004; Cerrone et al., 2021). Furthermore, the entire terrace sequence of the Crotona peninsula, near the Sila Massif, is affected by extensive normal faulting and lies on a well-studied megalandslide gliding toward the Ionian sea (*e.g.*, Mangano et al., 2020; Minelli et al., 2013; Zecchin et al., 2018), which could justify the lower elevation (Figure S1 in Supporting

**Figure 11.** Schematic evolution of the Pollino range and surrounding intermontane basins. (a) Paleo-topography and drainage pattern during the late Pliocene—early Pleistocene. The Campotenese and Mercure basins are characterized by NE direct drainage toward the Sant’Arcangelo basin (Filice & Seeber, 2019; Robustelli et al., 2014). (b) Increase in uplift rates with the onset of headward erosion (upstream migration of non-lithological knickpoints), extension mostly along NW striking structures, and endorheic conditions (lacustrine succession) in the intermontane basins. Noteworthy, the formation of wind gaps in the northern border of the Mercure and Campotenese basins. (c) Endorheic-exorheic transition of the Mercure basin and upstream propagation of knickpoints. (d) Endorheic-exorheic transition of the Campotenese and Castrovillari basins due to headward erosion and/or lake overspill with the onset of migration of minor knickpoints from the local drainage divide (after Robustelli et al., 2014). (e) Present-day configuration with fluvial dissection of the basin infill deposits caused by upstream migration of minor knickpoints. (2) Castrovillari basin; (3) Campotenese basin; (4) Mercure basin.

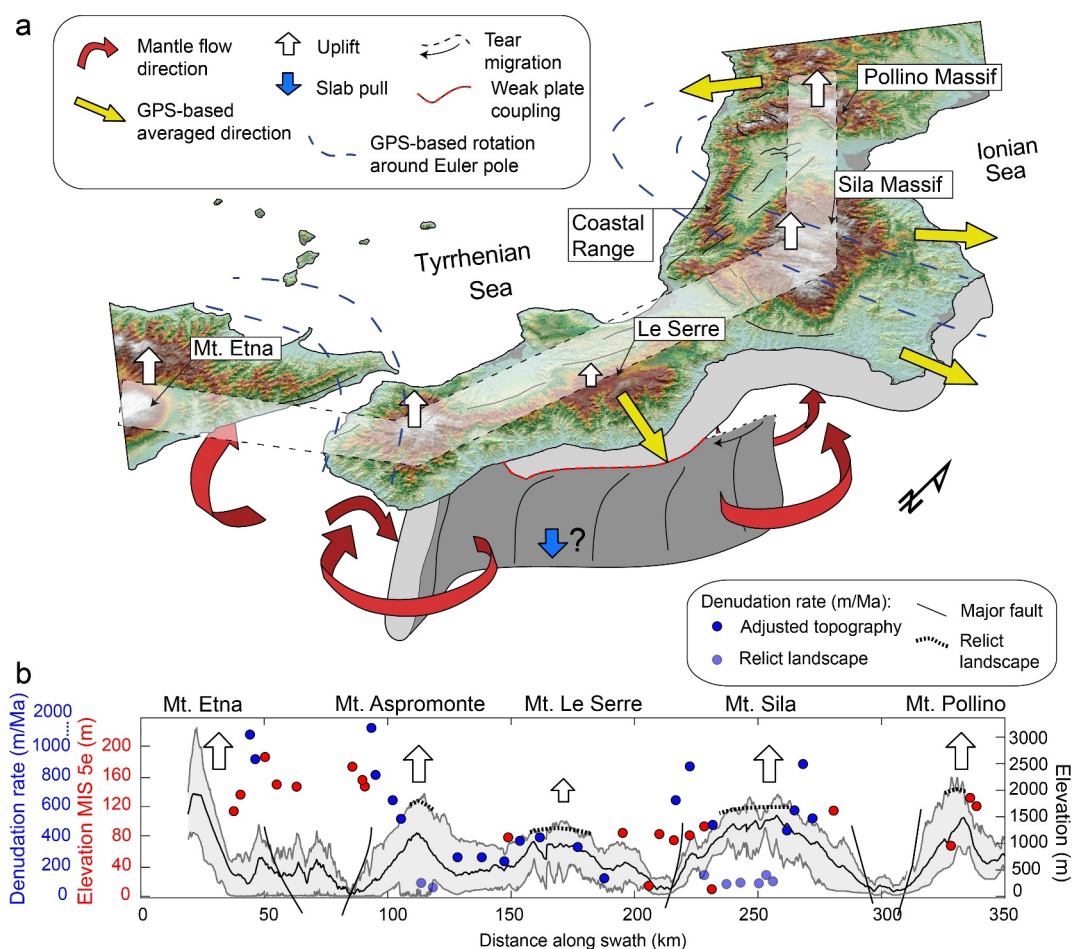


**Figure 12.** (a) Schematic representation of the topography and subduction zone of the southern Apennines and Calabria region Arc (after Civello & Margheriti, 2004; Faccenna et al., 2011; Gvirtzman & Nur, 1999; Palano et al., 2017). The pattern of mantle flow (red arrows) at the retreating slab edges promotes the large-scale Plio-Quaternary uplift in the Sila and Pollino Massif on the upper plate (white arrows). GPS-based direction and rotation around Euler pole are in yellow and dashed blue lines (after Palano et al., 2017). The uplift and faulting occur mostly at the same time, triggered and sustained by toroidal mantle flow through the slab windows. (b) Topographic swath profile (30 km window) with MIS 5e (after Ferranti et al., 2006) and data of basin-wide denudation rates (after Cyr et al., 2014; Olivetti et al., 2012; Roda-Boluda et al., 2019).

Information S1; 90–110 m; Nalin et al., 2020) of the MIS 5e terraces at this location with respect to those in the Pollino area (Figure S1 in Supporting Information S1; 114–125 m; Santoro et al., 2009). Therefore, further investigation is needed before considering this line of evidence with confidence.

Basin-wide denudation rates are up to 1,000 m/Myr in the Sila, Aspromonte and Etna areas (Figure 12b; Cyr et al., 2014; Olivetti et al., 2012) and decrease abruptly along the flanks of the Le Serre Massif (downstream of non-lithological knickpoints; Roda-Boluda et al., 2019). Given that the landscape lowering is balanced by the present-day uplift conditions, the different denudation rates indicate that the two regions have been adjusting to different magnitudes of uplift (gradually lower toward the Le Serre Massif; Figure 12b). This may in turn reflect the second long wavelength uplift phase, acting since the middle Pleistocene.

Although still widely debated, two types of mechanisms can be considered in the Calabrian subduction setting: (a) shallow scale processes related to crustal underplating and thickening of the forearc crust (Caputo et al., 2010; Ferranti et al., 2009; Minelli & Faccenna, 2010); (b) deep scale processes due to rebound after slab break-off (Buiter et al., 2002; Duretz & Gerya, 2013) or slab - upper plate decoupling (Gvirtzman & Nur, 1999, 2001) and/or upwelling related to toroidal flow within a slab window, formed following slab break-off (Faccenna et al., 2005, 2011; Palano et al., 2017). In the following paragraphs, we discuss the potential role of the aforementioned mechanisms in the development and support of the topography in the Calabrian Arc subduction zone.

The rejuvenation of topography can be driven by deep accretion at the base of the forearc crust, as observed in other subduction settings, such as Cascadia (Darin et al., 2022; Menant et al., 2020), Crete (Ott et al., 2019). This process can explain the rapid increase in surface uplift, high topography and extensional crustal deformation (Darin et al., 2022). In our setting, tectonic underplating can play a role in the topographic growth of the Le Serre - Sila Massif and the accretionary wedge offshore (Caputo et al., 2010; Ferranti et al., 2009). However, this process alone may not explain the along-strike, long wavelength uplift affecting the northern and southern sectors of the subduction zone, where compressional deformation terminated before the onset of large-scale uplift (Chiarabba et al., 2005; Tropeano et al., 2002).

Slab break-off could be considered the driving mechanism of the uplift of the Apennines and at least part of the Calabrian Arc, as it produces a sharp topographic and surface uplift signal, inducing a rapid isostatic rebound at timescales of  $10^4$  years (Duret & Gerya, 2013; Garzanti et al., 2018). In the areas of Sila, Pollino Massif and Sicily, slab break-off is supported by the lack of shallow high-velocity anomaly and the lack of seismicity (D'Agostino & Selvaggi, 2004; Chiarabba et al., 2005), which indicate the absence of a deep subducting slab. At the Calabrian-Sicily corner, SKS splitting data suggest a pattern of mantle flow around the narrow southern edge of the Calabrian slab and possibly also the northern one (Civello & Margheriti, 2004; Faccenna et al., 2011; Funicello et al., 2006; Palano et al., 2017; Piromallo & Morelli, 2003). The volcanism associated with Mt. Etna, in northern Sicily, is located on top of an uplifted region and presents alkaline magmatism that can be attributed to the rising of asthenospheric material through a slab window (Barreca et al., 2020; Faccenna et al., 2011) or along the plate contact (Gvirtzman & Nur, 1999, 2001). Interestingly, the beginning of Etna volcanism at about 500 ka is consistent with the onset of uplift in the Sila and Pollino ranges between 400 and 800 ka, suggesting a possible coeval mechanism of uplift and lateral tearing of the Calabrian slab to the south and to the north. Thus, the southeastward propagation of regional uplift, and extensional tectonics can be attributed to the process of mantle upwelling through a slab window, and related toroidal flow at the slab edge (Figure 12a; Faccenna et al., 2005, 2011). However, this process is inconsistent with the presence, beneath the Le Serre Massif, of a continuous slab, as indicated by the occurrence of deep seismicity (Calo et al., 2013; Faccenna et al., 2011; Neri et al., 2009; Piromallo & Morelli, 2003). In this context, the uplift of Le Serre Massif may result from weak plate coupling due to the extreme narrowing of the Calabrian slab (Figure 12a; Gvirtzman & Nur, 2001). A detailed knowledge of the crustal and mantle structures is necessary to distinguish between the possible acting processes and uplift-driving mechanisms. In addition, a more systematic age dating of uplifted marine terraces would contribute to a better understanding of the uplift trends, particularly along the coast of the Le Serre Massif.

The gradual transition of uplift trends from the southern Apennines to Calabria suggests a unique process at work, possibly related to disruption and narrowing of the slab linked to mantle dynamics. Our topographic and geomorphic analysis favors the model of slab detachment and decoupling followed by upwelling of the asthenospheric mantle, which can be associated with toroidal flow around the subducting Ionian slab. The link between regional uplift and extensional tectonics, currently active on the Southern Apennines, may be interpreted as surface response of slab break off, as proposed for the Central Apennines (Faccenna et al., 2011; Fellin et al., 2022; Lanari, Reitano, et al., 2023).

## 6. Conclusions

We reconstruct the evolution of topography at the convergent margin of the Calabrian Arc in the Southern Apennines. The area is a key setting within the Mediterranean region where surface deformation, subduction and volcanism coexist, producing a complex topography characterized by transient geomorphic features (e.g., knickpoints, marine and fluvial terraces and erosional surfaces). Our findings allow us to decipher the process that drove the recent topographic rejuvenation. At the short spatial scale, the evolution of topographic relief and formation, sedimentation and opening of intermontane basins is strongly controlled by the recent increase in rock-uplift and faulting activity in the Southern Apennines. Geomorphic features and knickpoints distribution indicate that the Pollino and Sila Massifs preserved an uplifted relict landscape that predates the age pulse of regional uplift. The timing of endorheic-exoreic transition is well-constrained in the Mercure basin at least post 500 ka. On the other hand, in Campotenese and Castrovillari basins, neither stratigraphic nor absolute ages are available. However, we can attribute their closure to the normal faulting activity that is approximately coeval with the topographic rejuvenation process. At the large scale, regional uplift can be driven by crustal underplating at the Le Serre Massif and by mantle upwelling in the Pollino-Sila starting between 400 and 800 ka. However, we can also consider a unique process of progressive lateral slab break-off and tearing, weak plate coupling and inflow of

asthenospheric mantle from Pollino, Sila to Le Serre Massif to explain the decrease of uplift magnitude from north to south and extensional tectonics. Interestingly, similar rates and timing of uplift has been observed in the southern counterpart of the Calabrian-Arc (Aspromonte, Peloritani and Etna range in Sicily), suggesting a possible coeval mechanism of slab tearing following by lateral inflow of mantle material.

## Data Availability Statement

The Shuttle Radar Topography Mission (SRTM) obtained elevation data are provided by OpenTopography (<https://doi.org/10.5069/G9445JDF>). All Supporting Information files and data are available from the OSF repository at <https://osf.io/b7uah/> (Clementucci et al., 2024). Structural and fluvial data are provided in Tables S1–S4 in Supporting Information S1, and marine terraces are summarized in Figure S1 in Supporting Information S1.

## Acknowledgments

This study was supported by the PhD School of Roma Tre and grant “Vinci 2020” awarded to RC (Number: C2-1403). The study was supported by the MIUR (Ministry of Education University and Research), Excellence Department Initiative, Art. 1, com. 314–337, Low 232/2016. And by PRIN 2017–2020 (Geodynamics of the Arabia-Eurasia collisional zones, PI C. Faccenna). We acknowledge the reviewers Frank J. Pazzaglia and anonymous Reviewer for their comments and criticism that improve the manuscript and the editor Duna Roda-Boluda and Susan Townsend. We thank C. Bazzucchi, G. Siravo, and E. Conrad for fieldwork support and G. Vance for revising the manuscript before submission. Open access funding provided by Eidgenössische Technische Hochschule Zurich.

## References

- Amato, A., & Cinque, A. (1999). Erosional landsurfaces of the Campano-Lucano Apennines (S. Italy): Genesis, evolution, and tectonic implications. *Tectonophysics*, 315(1–4), 251–267. [https://doi.org/10.1016/S0040-1951\(99\)00288-7](https://doi.org/10.1016/S0040-1951(99)00288-7)
- Antonoli, F., Ferranti, L., Lambeck, K., Kershaw, S., Verrubbi, V., & Dai Pra, G. (2006). Late Pleistocene to Holocene record of changing uplift rates in southern Calabria and northeastern Sicily (southern Italy, Central Mediterranean Sea). *Tectonophysics*, 422(1–4), 23–40. <https://doi.org/10.1016/j.tecto.2006.05.003>
- Ascione, A., Ciarcia, S., di Donato, V., Mazzoli, S., & Vitale, S. (2012). The Pliocene-Quaternary wedge-top basins of southern Italy: An expression of propagating lateral slab tear beneath the Apennines. *Basin Research*, 24(4), 456–474. <https://doi.org/10.1111/j.1365-2117.2011.00534.x>
- Ascione, A., & Cinque, A. (1999). Tectonics and erosion in the long term relief history of the Southern Apennines (Italy). *Zeitschrift für Geomorphologie, Supplement Band*, 117, 1–15.
- Barreca, G., Branca, S., Corsaro, R. A., Scarfi, L., Cannavò, F., Aloisi, M., et al. (2020). Slab detachment, mantle flow, and crustal collision in eastern Sicily (southern Italy): Implications on Mount Etna volcanism. *Tectonics*, 39(9), e2020TC006188. <https://doi.org/10.1029/2020TC006188>
- Beaumont, C., Muñoz, J. A., Hamilton, J., & Fullsack, P. (2000). Factors controlling the Alpine evolution of the central Pyrenees inferred from a comparison of observations and geodynamical models. *Journal of Geophysical Research*, 105(B4), 8121–8145. <https://doi.org/10.1029/1999JB900390>
- Bigi, G., Castellarin, A., Catalano, R., Coli, M., Cosentino, D., Dal Piaz, G. V., et al. (1989). Synthetic structural-kinematic map of Italy. *scale 1:2.000.000. CNR, Progetto Finalizzato Geodinamica Roma*.
- Bonardi, G., Amore, F. O., Ciampo, G., De Capoa, P., Miconnet, P., & Perrone, V. (1988). Il Complesso Liguride Auct.: stato delle conoscenze e problemi aperti sulla sua evoluzione preappenninica ed i suoi rapporti con l'arco calabro. *Memorie della Società Geologica Italiana*, 41, 17–35.
- Bonardi, G., Cavazza, W., Perrone, V., & Rossi, S. (2001). Calabria-Peloritani terrane and northern Ionian sea. *Anatomy of an orogen: The Apennines and adjacent Mediterranean basins*, 287–306. [https://doi.org/10.1007/978-94-015-9829-3\\_17](https://doi.org/10.1007/978-94-015-9829-3_17)
- Brozzetti, F., Cirillo, D., de Nardis, R., Cardinali, M., Lavecchia, G., Orecchio, B., et al. (2017a). Newly identified active faults in the Pollino seismic gap, southern Italy, and their seismotectonic significance. *Journal of Structural Geology*, 94, 13–31. <https://doi.org/10.1016/j.jsg.2016.10.005>
- Brozzetti, F., Cirillo, D., Liberi, F., PiLuso, E., Faraca, E., De Nardis, R., & Lavecchia, G. (2017b). Structural style of Quaternary extension in the Crati Valley (Calabrian Arc): Evidence in support of an east-dipping detachment fault. *Italian Journal of Geosciences*, 136(3), 434–453. <https://doi.org/10.3301/IJG.2017.11>
- Brozzetti, F., Lavecchia, G., Mancini, G., Milana, G., & Cardinali, M. (2009). Analysis of the 9 September 1998 Mw 5.6 Mercure earthquake sequence (Southern Apennines, Italy): A multidisciplinary approach. *Tectonophysics*, 476(1–2), 210–225. <https://doi.org/10.1016/j.tecto.2008.12.007>
- Buiter, S. J., Govers, R., & Wortel, M. J. R. (2002). Two-dimensional simulations of surface deformation caused by slab detachment. *Tectonophysics*, 354(3–4), 195–210. [https://doi.org/10.1016/S0040-1951\(02\)00336-0](https://doi.org/10.1016/S0040-1951(02)00336-0)
- Calo, M., Parisi, L., & Luzio, D. (2013). Lithospheric P- and S-wave velocity models of the Sicilian area using WAM tomography: Procedure and assessments. *Geophysical Journal International*, 195(1), 625–649. <https://doi.org/10.1093/gji/ggt252>
- Capalbo, A., Ascione, A., Aucelli, P., & Mazzoli, S. (2010). Valutazione del tasso di erosione in Appennino Meridionale da dati geologico-geomorfologici. *Alpine and Mediterranean Quaternary*, 23(1), 75–90.
- Caputo, R., Bianca, M., & D'Onofrio, R. (2010). Ionian marine terraces of southern Italy: Insights into the Quaternary tectonic evolution of the area. *Tectonics*, 29(4). <https://doi.org/10.1029/2009TC002625>
- Carminati, E., Lustrino, M., & Doglioni, C. (2012). Geodynamic evolution of the central and western Mediterranean: Tectonics vs. igneous petrology constraints. *Tectonophysics*, 579, 173–192. <https://doi.org/10.1016/j.tecto.2012.01.026>
- Carobene, L. (2003). Genesi, età, sollevamento ed erosione dei terrazzi marini di Crosia-Calopezzati (Costa Ionica della Calabria-Italia). *Italian Journal of Quaternary Sciences*, 16, 43–90.
- Catalano, S., Monaco, C., Tortorici, L., Paltrinieri, W., & Steel, N. (2004). Neogene-Quaternary tectonic evolution of the southern Apennines. *Tectonics*, 23(2). <https://doi.org/10.1029/2003TC001512>
- Catalano, S., Monaco, C., Tortorici, L., & Tansi, C. (1993). Pleistocene strike-slip tectonics in the Lucanian Apennine (Southern Italy). *Tectonics*, 12(3), 656–665. <https://doi.org/10.1029/92TC02251>
- Cerrone, C., Vacchi, M., Fontana, A., & Rovere, A. (2021). Last Interglacial sea-level proxies in the Western Mediterranean. *Earth System Science Data*, 13(9), 4485–4527. <https://doi.org/10.5194/essd-13-4485-2021>
- Chiarabba, C., Jovane, L., & DiStefano, R. (2005). A new view of the Italian seismicity using 20 years of instrumental recordings. *Tectonophysics*, 395(3–4), 251–268. <https://doi.org/10.1016/j.tecto.2004.09.013>
- Chiarella, D., Capella, W., Longhitano, S. G., & Muto, F. (2021). Fault-controlled base-of-scarp deposits. *Basin Research*, 33(2), 1056–1075. <https://doi.org/10.1111/bre.12505>



- Cifelli, F., Mattei, M., & Rossetti, F. (2007). Tectonic evolution of arcuate mountain belts on top of a retreating subduction slab: The example of the Calabrian Arc. *Journal of Geophysical Research*, *112*(9). <https://doi.org/10.1029/2006JB004848>
- Cinque, A., Patacca, E., Scandone, P., & Tozzi, M. (1993). Quaternary kinematic evolution of the Southern Apennines. Relationships between surface geological features and deep lithospheric structures. *Annali di Geofisica*, *36*(2), 249–260. <https://doi.org/10.4401/ag-4283>
- Cinti, F. R., Cucci, L., Pantosti, D., D'Addezio, G., & Meghraoui, M. (1997). A major seismogenic fault in a 'silent area': The Castrovillari fault (southern Apennines, Italy). *Geophysical Journal International*, *130*(3), 595–605. <https://doi.org/10.1111/j.1365-246X.1997.tb01855.x>
- Cinti, F. R., Moro, M., Pantosti, D., Cucci, L., & D'addezio, G. (2002). New constraints on the seismic history of the Castrovillari fault in the Pollino gap (Calabria, southern Italy). *Journal of Seismology*, *6*(2), 199–217. <https://doi.org/10.1023/A:1015693127008>
- Cirillo, D., Totaro, C., Lavecchia, G., Orecchio, B., de Nardis, R., Presti, D., et al. (2022). Structural complexities and tectonic barriers controlling recent seismic activity in the Pollino area (Calabria–Lucania, southern Italy) – Constraints from stress inversion and 3D fault model building. *Solid Earth*, *13*(1), 205–228. <https://doi.org/10.5194/se-13-205-2022>
- Civello, S., & Margheriti, L. (2004). Toroidal mantle flow around the Calabrian slab (Italy) from SKS splitting. *Geophysical Research Letters*, *31*(10). <https://doi.org/10.1029/2004GL019607>
- Clementucci, R., Ballato, P., Siame, L., Fox, M., Lanari, R., Sembroni, A., et al. (2023a). Surface uplift and topographic rejuvenation of a tectonically inactive range: Insights from the Anti-Atlas and the Siroua Massif (Morocco). *Tectonics*, *42*(2), e2022TC007383. <https://doi.org/10.1029/2022TC007383>
- Clementucci, R., Ballato, P., Siame, L. L., Faccenna, C., Racano, S., Torreti, G., et al. (2023b). Transient response to changes in uplift rates in the northern Atlas-Meseta system (Morocco). *Geomorphology*, *108765*, 108765. <https://doi.org/10.1016/j.geomorph.2023.108765>
- Clementucci, R., Ballato, P., Siame, L. L., Faccenna, C., Yaaqoub, A., Essaifi, A., et al. (2022). Lithological control on topographic relief evolution in a slow tectonic setting (Anti-Atlas, Morocco). *Earth and Planetary Science Letters*, *596*, 117788. <https://doi.org/10.1016/j.epsl.2022.117788>
- Clementucci, R., Lanari, R., Faccenna, C., Crosetto, S., Reitano, R., Zoppis, G., & Ballato, P. (2024). Supporting data of Morpho-tectonic evolution of southern Apennines: Insights from Pollino range and surrounding intermountain basins. [Dataset]. *OSF HOME*. <https://doi.org/10.17605/OSF.IO/B7UAH>
- Colella, A. (1988). Fault-controlled marine Gilbert-type fan deltas. *Geology*, *16*(11), 1031–1034. [https://doi.org/10.1130/0091-7613\(1988\)016<1031:FCMGTF>2.3.CO;2](https://doi.org/10.1130/0091-7613(1988)016<1031:FCMGTF>2.3.CO;2)
- Colella, A., De Boer, P. L., & Nio, S. D. (1987). Sedimentology of a marine intermontane Pleistocene Gilbert-type fan-delta complex in the Crati Basin, Calabria, southern Italy. *Sedimentology*, *34*(4), 721–736. <https://doi.org/10.1111/j.1365-3091.1987.tb00798.x>
- Corbi, F., Fubelli, G., Lucà, F., Muto, F., Pelle, T., Robustelli, G., et al. (2009). Vertical movements in the Ionian margin of the Sila Massif (Calabria, Italy). *Bollettino della Società Geologica Italiana*, *128*(3), 731–738. <https://doi.org/10.3301/IJG.2009.128.3.731>
- Corrado, S., Aldega, L., di Leo, P., Giampaolo, C., Invernizzi, C., Mazzoli, S., & Zattin, M. (2005). Thermal maturity of the axial zone of the southern Apennines fold-and-thrust belt (Italy) from multiple organic and inorganic indicators. *Terra Nova*, *17*(1), 56–65. <https://doi.org/10.1111/j.1365-3121.2004.00584.x>
- Cowie, P., Phillips, R., Roberts, G., McCaffrey, K., Zijerveld, L. J. J., Gregory, L. C., et al. (2017). Orogen-scale uplift in the central Italian Apennines drives episodic behaviour of earthquake faults. *Scientific Reports*, *7*(1), 44858. <https://doi.org/10.1038/srep44858>
- Cramer, F., Lithgow-Bertelloni, C. R., & Tackley, P. J. (2017). The dynamical control of subduction parameters on surface topography. *Geochemistry, Geophysics, Geosystems*, *18*(4), 1661–1687. <https://doi.org/10.1002/2017GC006821>
- Cucci, L. (2004). Raised marine terraces in the Northern Calabrian Arc (Southern Italy): A ~ 600 kyr-long geological record of regional uplift. *Annals of Geophysics*, *47*(4). <https://doi.org/10.4401/ag-3350>
- Cucci, L., & Cinti, F. R. (1998). TECTONOPHYSICS I Regional uplift and local tectonic deformation recorded by the Quaternary marine terraces on the Ionian coast of northern Calabria (southern Italy). *Tectonophysics*, *292*(1–2), 67–83. [https://doi.org/10.1016/s0040-1951\(98\)00061-4](https://doi.org/10.1016/s0040-1951(98)00061-4)
- Cuffaro, M., Riguzzi, F., Scrocca, D., & Doglioni, C. (2011). Coexisting tectonic settings: The example of the southern Tyrrhenian Sea. *International Journal of Earth Sciences*, *100*(8), 1915–1924. <https://doi.org/10.1007/s00531-010-0625-z>
- Cyr, A. J., Granger, D. E., Olivetti, V., & Molin, P. (2014). Distinguishing between tectonic and lithologic controls on bedrock channel longitudinal profiles using cosmogenic <sup>10</sup>Be erosion rates and channel steepness index. *Geomorphology*, *209*, 27–38. <https://doi.org/10.1016/j.geomorph.2013.12.010>
- D'Agostino, N., England, P., Hunstad, I., & Selvaggi, G. (2014). Gravitational potential energy and active deformation in the Apennines. *Earth and Planetary Science Letters*, *397*, 121–132. <https://doi.org/10.1016/j.epsl.2014.04.013>
- D'Agostino, N., & Selvaggi, G. (2004). Crustal motion along the Eurasia-Nubia plate boundary in the Calabrian Arc and Sicily and active extension in the Messina Straits from GPS measurements. *Journal of Geophysical Research*, *109*(B11). <https://doi.org/10.1029/2004JB002998>
- Darin, M. H., Armentrout, J. M., & Dorsey, R. J. (2022). Oligocene onset of uplift and inversion of the Cascadia forearc basin, southern Oregon Coast Range, USA. *Geology*, *50*(5), 603–609. <https://doi.org/10.1130/G49925.1>
- Dijk, J. P., Bello, M., Brancaloni, G. P., Cantarella, G., Costa, V., Frixia, A., et al. (2000). A regional structural model for the northern sector of the Calabrian Arc (southern Italy). *Tectonophysics*, *324*(4), 267–320. [https://doi.org/10.1016/s0040-1951\(00\)00139-6](https://doi.org/10.1016/s0040-1951(00)00139-6)
- Duretz, T., & Gerya, T. v. (2013). Slab detachment during continental collision: Influence of crustal rheology and interaction with lithospheric delamination. *Tectonophysics*, *602*, 124–140. <https://doi.org/10.1016/j.tecto.2012.12.024>
- Faccenna, C., & Becker, T. W. (2020). Topographic expressions of mantle dynamics in the Mediterranean. *Earth-Science Reviews*, *209*, 103327. <https://doi.org/10.1016/j.earscirev.2020.103327>
- Faccenna, C., Civetta, L., D'Antonio, M., Fucicello, F., Margheriti, L., & Piromallo, C. (2005). Constraints on mantle circulation around the deforming Calabrian slab. *Geophysical Research Letters*, *32*(6), 1–4. <https://doi.org/10.1029/2004GL021874>
- Faccenna, C., Molin, P., Orecchio, B., Olivetti, V., Bellier, O., Fucicello, F., et al. (2011). Topography of the Calabria subduction zone (southern Italy): Clues for the origin of Mt. Etna. *Tectonics*, *30*(1). <https://doi.org/10.1029/2010TC002694>
- Faccenna, C., Piromallo, C., Crespo-Blanc, A., Jolivet, L., & Rossetti, F. (2004). Lateral slab deformation and the origin of the western Mediterranean arcs. *Tectonics*, *23*(1). <https://doi.org/10.1029/2002TC001488>
- Faure Walker, J., Roberts, G. P., Cowie, P. A., Papanikolaou, I., Michetti, A. M., Sammonds, P., et al. (2012). Relationship between topography, rates of extension and mantle dynamics in the actively-extending Italian Apennines. *Earth and Planetary Science Letters*, *325*, 76–84. <https://doi.org/10.1016/j.epsl.2012.01.028>
- Fellini, M. G., Jose, M. S., Faccenna, C., Willett, S. D., Cosentino, D., Lanari, R., et al. (2022). Transition from slab roll-back to slab break-off in the central Apennines, Italy: Constraints from the stratigraphic and thermochronologic record. *Bulletin*, *134*(7–8), 1916–1930. <https://doi.org/10.1130/B36123.1>
- Ferranti, L., Antonioli, F., Mauz, B., Amorosi, A., Dai Pra, G., Mastroruzzi, G., et al. (2006). Markers of the last interglacial sea-level high stand along the coast of Italy: Tectonic implications. *Quaternary International*, *145–146*, 30–54. <https://doi.org/10.1016/j.quaint.2005.07.009>

- Ferranti, L., Santoro, E., Mazzella, M. E., Monaco, C., & Morelli, D. (2009). Active transposition in the northern Calabria Apennines, southern Italy. *Tectonophysics*, 476(1–2), 226–251. <https://doi.org/10.1016/j.tecto.2008.11.010>
- Filice, F., & Seeber, L. (2019). The Culmination of an Oblique Time-Transgressive Arc Continent Collision: The Pollino Massif Between Calabria and the Southern Apennines, Italy. *Tectonics*, 38(8), 3261–3280. <https://doi.org/10.1029/2017TC004932>
- Fisher, J. A., Pazzaglia, F. J., Anastasio, D. J., & Gallen, S. F. (2022). Linear inversion of fluvial topography in the northern Apennines: Comparison of base-level fall to crustal shortening. *Tectonics*, 41(11), e2022TC007379. <https://doi.org/10.1029/2022tc007379>
- Flint, J. J. (1974). Stream gradient as a function of order, magnitude, and discharge. *Water Resources Research*, 10(5), 969–973. <https://doi.org/10.1029/WR010i005p0969>
- Forte, A. M., & Whipple, K. X. (2019). Short communication: The Topographic Analysis Kit (TAK) for TopoToolbox. *Earth Surface Dynamics*, 7(1), 87–95. <https://doi.org/10.5194/esurf-7-87-2019>
- Funicello, F., Moroni, M., Piromallo, C., Faccenna, C., Cenedese, A., & Bui, H. A. (2006). Mapping mantle flow during retreating subduction: Laboratory models analyzed by feature tracking. *Journal of Geophysical Research*, 111(B3). <https://doi.org/10.1029/2005JB003792>
- Gallen, S. F., Seymour, N. M., Glotzbach, C., Stockli, D. F., & O'Sullivan, P. (2023). Calabrian forearc uplift paced by slab–mantle interactions during subduction retreat. *Nature Geoscience*, 16(6), 1–8. <https://doi.org/10.1038/s41561-023-01185-4>
- Garzanti, E., Radeff, G., & Malusà, M. G. (2018). Slab breakoff: A critical appraisal of a geological theory as applied in space and time. *Earth-Science Reviews*, 177, 303–319. <https://doi.org/10.1016/j.earscirev.2017.11.012>
- GE M. I. N. A. (1963). Il bacino del Mercure. In: *Ligniti e torbe dell'Italia continentale* (Ed. by GE.MI.NA.), (pp. 137–156). Società Geomineraria Nazionale.
- Geurts, A. H., Whittaker, A. C., Gawthorpe, R. L., & Cowie, P. A. (2020). Transient landscape and stratigraphic responses to drainage integration in the actively extending central Italian Apennines. *Geomorphology*, 353, 107013. <https://doi.org/10.1016/j.geomorph.2019.107013>
- Ghisetti, F., & Vezzani, L. (1983). Structural map of Mt. Pollino (Southern Italy). S.EL.CA., Firenze, scale 1:50.000. 1 sheet. Scale.
- Gioia, D., Corrado, G., Danese, M., Minervino Amodio, A., & Schiattarella, M. (2023). Post-lacustrine evolution of a tectonically-controlled intermontane basin: Drainage network analysis of the Mercure basin, southern Italy. *Frontiers in Earth Science*, 11, 1112067. <https://doi.org/10.3389/feart.2023.1112067>
- Gioia, D., Schiattarella, M., Mattei, M., & Nico, G. (2011). Quantitative morphotectonics of the Pliocene to Quaternary Auletta basin, southern Italy. *Geomorphology*, 134(3–4), 326–343. <https://doi.org/10.1016/j.geomorph.2011.07.009>
- Goren, L., Fox, M., & Willett, S. D. (2014). Tectonics from fluvial topography using formal linear inversion: Theory and applications to the Inyo Mountains, California. *Journal of Geophysical Research: Earth Surface*, 119(8), 1651–1681. <https://doi.org/10.1002/2014JF003079>
- Guillaume, B., Moroni, M., Funicello, F., Martinod, J., & Faccenna, C. (2010). Mantle flow and dynamic topography associated with slab window opening: Insights from laboratory models. *Tectonophysics*, 496(1–4), 83–98. <https://doi.org/10.1016/j.tecto.2010.10.014>
- Gvirtzman, Z., & Nur, A. (1999). The formation of Mount Etna as the consequence of slab rollback. *Nature*, 401(6755), 782–785. <https://doi.org/10.1038/44555>
- Gvirtzman, Z., & Nur, A. (2001). Residual topography, lithospheric structure and sunken slabs in the central Mediterranean. *Earth and Planetary Science Letters*, 187(1–2), 117–130. [https://doi.org/10.1016/S0012-821X\(01\)00272-2](https://doi.org/10.1016/S0012-821X(01)00272-2)
- Hack, J. T. (1957). *Studies of longitudinal stream profiles in Virginia and Maryland* (Vol. 294). US Government Printing Office. <https://doi.org/10.3133/pp294b>
- Heidarzadeh, G., Ballato, P., Hassanzadeh, J., Ghassemi, M. R., & Strecker, M. R. (2017). Lake overflow and onset of fluvial incision in the Iranian Plateau: Insights from the Mianeh Basin. *Earth and Planetary Science Letters*, 469, 135–147. <https://doi.org/10.1016/j.epsl.2017.04.019>
- Hippolyte, J. C., Angelier, J., & Roure, F. B. (1994). A major geodynamic change revealed by Quaternary stress patterns in the Southern Apennines (Italy). *Tectonophysics*, 230(3–4), 199–210. [https://doi.org/10.1016/0040-1951\(94\)90135-X](https://doi.org/10.1016/0040-1951(94)90135-X)
- Iannace, A., D'Errico, M., & Vitale, S. (2004). Carta Geologica dell'area compresa tra Maratea, Castrovillari e Sangineto. In S. Vitale & A. Iannace (Eds.), *Analisi Dello Strain Finito in 3D Dell'Unità Pollino-Ciagola (Confine Calabro-lucano, Italia Meridionale)*, *Studi Geologici Camerti, Nuova Serie* (Vol. 2, pp. 153–167).
- Invernizzi, C., Bigazzi, G., Corrado, S., Di Leo, P., Schiattarella, M., & Zattin, M. (2008). New thermobaric constraints on the exhumation history of the Liguride accretionary wedge, southern Italy. *Ofioliti*, 33(1), 21–32. <https://doi.org/10.4454/ofioliti.v33i1.357>
- Kirby, E., & Whipple, K. X. (2012). Expression of active tectonics in erosional landscapes. *Journal of Structural Geology*, 44, 54–75. <https://doi.org/10.1016/j.jsg.2012.07.009>
- Knott, S. D., & Turco, E. (1991). Late Cenozoic kinematics of the Calabrian arc, southern Italy. *Tectonics*, 10(6), 1164–1172. <https://doi.org/10.1029/91TC01535>
- Lanari, R., Boutoux, A., Faccenna, C., Herman, F., Willett, S. D., & Ballato, P. (2023). Cenozoic exhumation in the Mediterranean and the Middle East. *Earth-Science Reviews*, 237, 104328. <https://doi.org/10.1016/j.earscirev.2023.104328>
- Lanari, R., Faccenna, C., Benedetti, L., Sembroni, A., Bellier, O., Menichelli, I., et al. (2021). Formation and Persistence of Extensional Internally Drained Basins: The Case of the Fucino Basin (Central Apennines, Italy). *Tectonics*, 40(6). <https://doi.org/10.1029/2020TC006442>
- Lanari, R., Reitano, R., Faccenna, C., Ballato, P., & Piana Agostinetti, N. (2023). Surface response to deep subduction dynamics: Insight from the Apennines, Italy. *Tectonics*, 42(3). <https://doi.org/10.1029/2022TC007461>
- Lavecchia, G., Bello, S., Andrenacci, C., Cirillo, D., Pietrolungo, F., Talone, D., et al. (2024). QUIN 2.0-new release of the QUaternary fault strain Indicators database from the Southern Apennines of Italy. *Scientific Data*, 11(1), 189. <https://doi.org/10.1038/s41597-024-03008-6>
- Liberi, F., & Piluso, E. (2009). Tectonometamorphic evolution of the ophiolitic sequences from Northern Calabrian Arc. *Bollettino della Società Geologica Italiana*, 128(2), 483–493. <https://doi.org/10.3301/IJG.2009.128.2.483>
- Lucà, F., Brogno, A., Tripodi, V., & Robustelli, G. (2022). Terrace Morpho-Sedimentary Sequences on the Sibari Plain (Calabria, Southern Italy): Implication for Sea Level and Tectonic Controls. *Geosciences*, 12(5), 211. <https://doi.org/10.3390/geosciences12050211>
- Maesano, F. E., Tiberti, M. M., & Basili, R. (2017). The Calabrian Arc: Three-dimensional modelling of the subduction interface. *Scientific Reports*, 7(1), 8887. <https://doi.org/10.1038/s41598-017-09074-8>
- Malinverno, A., & Ryan, W. B. (1986). Extension in the Tyrrhenian Sea and shortening in the Apennines as result of arc migration driven by sinking of the lithosphere. *Tectonics*, 5(2), 227–245. <https://doi.org/10.1029/TC005i002p0227>
- Mangano, G., Zecchin, M., & Civile, D. (2020). Large-scale gravity-driven phenomena in the Crotona Basin, southern Italy. *Marine and Petroleum Geology*, 117, 104386. <https://doi.org/10.1016/j.marpetgeo.2020.104386>
- Marder, E., Gallen, S. F., & Pazzaglia, F. J. (2023). Late Cenozoic deformation in the US southern Colorado Front Range revealed by river profile analysis and fluvial terraces. *Geological Society of America Bulletin*. <https://doi.org/10.1130/B36440.1>
- Mattei, M., Cifelli, F., & D'Agostino, N. (2007). The evolution of the Calabrian Arc: Evidence from paleomagnetic and GPS observations. *Earth and Planetary Science Letters*, 263(3–4), 259–274. <https://doi.org/10.1016/j.epsl.2007.08.034>

- Mattei, M., Speranza, F., Argentieri, A., Rossetti, F., Sagnotti, L., & Funicello, R. (1999). Extensional tectonics in the Amantea basin (Calabria, Italy): A comparison between structural and magnetic anisotropy data. *Tectonophysics*, 307(1–2), 33–49. [https://doi.org/10.1016/S0040-1951\(99\)00117-1](https://doi.org/10.1016/S0040-1951(99)00117-1)
- Mazzoli, S., D'Errico, M., Aldega, L., Corrado, S., Invernizzi, C., Shiner, P., & Zattin, M. (2008). Tectonic burial and “young” (<10 Ma) exhumation in the southern Apennines fold-and-thrust belt (Italy). *Geology*, 36(3), 243–246. <https://doi.org/10.1130/G24344A.1>
- Menant, A., Angiboust, S., Gerya, T., Lacassin, R., Simoes, M., & Grandin, R. (2020). Transient stripping of subducting slabs controls periodic forearc uplift. *Nature Communications*, 11(1), 1823. <https://doi.org/10.1038/s41467-020-15580-7>
- Meschis, M., Teza, G., Serpelloni, E., Elia, L., Lattanzi, G., di Donato, M., & Castellaro, S. (2022). Refining Rates of Active Crustal Deformation in the Upper Plate of Subduction Zones, Implied by Geological and Geodetic Data: The E-Dipping West Crati Fault, Southern Italy. *Remote Sensing*, 14(21), 5303. <https://doi.org/10.3390/rs14215303>
- Michetti, A. M., Ferrelli, L., Serva, L., & Vittori, E. (1997). Geological evidence for strong historical earthquakes in an “aseismic” region: The Pollino case (Southern Italy). *Journal of Geodynamics*, 24(1–4), 67–86. [https://doi.org/10.1016/S0264-3707\(97\)00018-5](https://doi.org/10.1016/S0264-3707(97)00018-5)
- Minelli, L., Billi, A., Faccenna, C., Gervasi, A., Guerra, I., Orecchio, B., & Speranza, G. (2013). Discovery of a gliding salt-detached megaslide, Calabria, Ionian Sea, Italy. *Geophysical Research Letters*, 40(16), 4220–4224. <https://doi.org/10.1002/grl.50818>
- Minelli, L., & Faccenna, C. (2010). Evolution of the Calabrian accretionary wedge (central Mediterranean). *Tectonics*, 29(4). <https://doi.org/10.1029/2009TC002562>
- Molin, P., Dramis, F., & Lupia Palmieri, E. (2002). *The Pliocene–Quaternary uplift of the Ionian northern Calabria coastal belt between Corigliano Calabro and Capo Triunto* (pp. 135–145). Studi Geologici Camerti. Volume Speciale.
- Molin, P., Pazzaglia, F. J., & Dramis, F. (2004). Geomorphic expression of active tectonics in a rapidly-deforming forearc, Sila Massif, Calabria, southern Italy. *American Journal of Science*, 304(7), 559–589. <https://doi.org/10.2475/ajs.304.7.559>
- Molli, G., Brogi, A., Caggianelli, A., Capezzuoli, E., Liotta, D., Spina, A., & Zibra, I. (2020). Late Palaeozoic tectonics in Central Mediterranean: A reappraisal. *Swiss Journal of Geosciences*, 113, 1–32. <https://doi.org/10.1186/s00015-020-00375-1>
- Monaco, C., Tortorici, L., & Paltrinieri, W. (1998). Structural evolution of the Lucanian Apennines, southern Italy. *Journal of Structural Geology*, 20(5), 617–638. [https://doi.org/10.1016/S0191-8141\(97\)00105-3](https://doi.org/10.1016/S0191-8141(97)00105-3)
- Montgomery, D. R., & Fofoula-Georgiou, E. (1993). Channel network source representation using digital elevation models. *Water Resources Research*, 29(12), 3925–3934. <https://doi.org/10.1029/93WR02463>
- Morisawa, M. E. (1962). Quantitative geomorphology of some watersheds in the Appalachian Plateau. *Geological Society of America Bulletin*, 73(9), 1025–1046. [https://doi.org/10.1130/00167606\(1962\)73\[1025:QGOSWI\]2.0.CO;2](https://doi.org/10.1130/00167606(1962)73[1025:QGOSWI]2.0.CO;2)
- Moumeni, M., Delchiaro, M., Della Seta, M., Nozaem, R., Ballato, P., Leonard, J. S., et al. (2023). Interplay between tectonics and surface processes in the evolution of mountain ranges: Insights from landscape dynamics, uplift, and active deformation of Talesh Mountains (NW Iranian Plateau margin). *Geomorphology*, 109029, 109029. <https://doi.org/10.1016/j.geomorph.2023.109029>
- Nalin, R., Lamothe, M., Auclair, M., & Massari, F. (2020). Chronology of the marine terraces of the Crotona Peninsula (Calabria, southern Italy) by means of infrared-stimulated luminescence (IRSL). *Marine and Petroleum Geology*, 122, 104645. <https://doi.org/10.1016/j.marpetgeo.2020.104645>
- Neri, G., Orecchio, B., Totaro, C., Falcone, G., & Presti, D. (2009). Subduction beneath Southern Italy close the ending: Results from seismic tomography. *Seismological Research Letters*, 80(1), 63–70. <https://doi.org/10.1785/gssrl.80.1.63>
- Ogniben, L. (1969). Schema introduttivo alla geologia del confine calabro-lucano. *Mem. Soc. Geol. It.*, 8, 453–763.
- Olivetti, V., Cyr, A. J., Molin, P., Faccenna, C., & Granger, D. E. (2012). Uplift history of the Sila Massif, southern Italy, deciphered from cosmogenic <sup>10</sup>Be erosion rates and river longitudinal profile analysis. *Tectonics*, 31(3). <https://doi.org/10.1029/2011TC003037>
- Olivetti, V., Laura, B. M., Claudio, F., & Stuart, F. M. (2017). Dating the topography through thermochronology: Application of Pecube code to inverted vertical profile in the eastern Sila Massif, southern Italy. *Italian Journal of Geosciences*, 136(3), 321–336. <https://doi.org/10.3301/IJG.2016.09>
- Ott, R. F., Gallen, S. F., Wegmann, K. W., Biswas, R. H., Herman, F., & Willett, S. D. (2019). Pleistocene terrace formation, Quaternary rock uplift rates and geodynamics of the Hellenic Subduction Zone revealed from dating of paleoshorelines on Crete, Greece. *Earth and Planetary Science Letters*, 525, 115757. <https://doi.org/10.1016/j.epsl.2019.115757>
- Oumet, W. B., Whipple, K. X., & Granger, D. E. (2009). Beyond threshold hillslopes: Channel adjustment to base-level fall in tectonically active mountain ranges. *Geology*, 37(7), 579–582. <https://doi.org/10.1130/G30013A.1>
- Palano, M., Piromallo, C., & Chiarabba, C. (2017). Surface imprint of toroidal flow at retreating slab edges: The first geodetic evidence in the Calabrian subduction system. *Geophysical Research Letters*, 44(2), 845–853. <https://doi.org/10.1002/2016GL071452>
- Papanikolaou, I. D., & Roberts, G. P. (2007). Geometry, kinematics and deformation rates along the active normal fault system in the southern Apennines: Implications for fault growth. *Journal of Structural Geology*, 29(1), 166–188. <https://doi.org/10.1016/j.jsg.2006.07.009>
- Patacca, E., Sartori, R., & Scandone, P. (1990). Tyrrhenian basin and Apenninic arcs: Kinematic relations since late Tortonian times. *Memorie della Società Geologica Italiana*, 45, 425–451.
- Patacca, E., & Scandone, P. (2007). Geology of the southern Apennines. *Bollettino della Società Geologica Italiana*, 7, 75–119.
- Pavano, F., & Gallen, S. F. (2021). A Geomorphic Examination of the Calabrian Forearc Translation. *Tectonics*, 40(7). <https://doi.org/10.1029/2020TC006692>
- Perron, J. T., & Royden, L. (2013). An integral approach to bedrock river profile analysis. *Earth Surface Processes and Landforms*, 38(6), 570–576. <https://doi.org/10.1002/esp.3302>
- Petit, J. P. (1987). Criteria for the sense of movement on fault surfaces in brittle rocks. *Journal of Structural Geology*, 9(5–6), 597–608. [https://doi.org/10.1016/0191-8141\(87\)90145-3](https://doi.org/10.1016/0191-8141(87)90145-3)
- Piromallo, C., & Morelli, A. (2003). P wave tomography of the mantle under the Alpine-Mediterranean area. *Journal of Geophysical Research*, 108(B2). <https://doi.org/10.1029/2002JB001757>
- Racano, S., Schildgen, T., Ballato, P., Yıldırım, C., & Wittmann, H. (2023). Rock-uplift history of the Central Pontides from river-profile inversions and implications for development of the North Anatolian Fault. *Earth and Planetary Science Letters*, 616, 118231. <https://doi.org/10.1016/j.epsl.2023.118231>
- Robustelli, G., Ermolli, E. R., Petrosino, P., Jicha, B., Sardella, R., & Donato, P. (2014). Tectonic and climatic control on geomorphological and sedimentary evolution of the Mercure basin, southern Apennines, Italy. *Geomorphology*, 214, 423–435. <https://doi.org/10.1016/j.geomorph.2014.02.026>
- Roda-Boluda, D. C., D'Arcy, M., Whittaker, A. C., Gheorghiu, D. M., & Rodés, Á. (2019). <sup>10</sup>Be erosion rates controlled by transient response to normal faulting through incision and landsliding. *Earth and Planetary Science Letters*, 507, 140–153. <https://doi.org/10.1016/j.epsl.2018.11.032>

- Roda-Boluda, D. C., & Whittaker, A. C. (2017). Structural and geomorphological constraints on active normal faulting and landscape evolution in Calabria, Italy. *Geological Society of London. Collection*, 174(4), 701–720. <https://doi.org/10.6084/m9.figshare.c.3689464.v2>
- Rossetti, F., Faccenna, C., Goffé, B., Monié, P., Argentieri, A., Funicello, R., & Mattei, M. (2001). Alpine structural and metamorphic signature of the Sila Piccola Massif nappe stack (Calabria, Italy): Insights for the tectonic evolution of the Calabrian Arc. *Tectonics*, 20(1), 112–133. <https://doi.org/10.1029/2000TC900027>
- Rovida, A., Camassi, R., Gasperini, P., & Stucchi, M. (2011). Catalogo parametrico dei terremoti italiani. *Tratto da*. <https://doi.org/10.6092/INGV.IT-CPT11>
- Royden, L., & Taylor Perron, J. (2013). Solutions of the stream power equation and application to the evolution of river longitudinal profiles. *Journal of Geophysical Research: Earth Surface*, 118(2), 497–518. <https://doi.org/10.1002/jgrf.20031>
- Royden, L. H. (1993). The tectonic expression slab pull at continental convergent boundaries. *Tectonics*, 12(2), 303–325. <https://doi.org/10.1029/92TC02248>
- Russo, F., & Schiattarella, M. (1992). Osservazioni preliminari sull'evoluzione morfostrutturale del bacino di Castrovillari (Calabria settentrionale). *Studi Geologici Camerti*, 1992(1), 271–278.
- Salvini. (2004). Daisy 3: The Structural Data Integrated System Analyzer. [Software]. University of Roma Tre.
- Santantonio, M., Fabbì, S., & Aldega, L. (2016). Mesozoic architecture of a tract of the European–Iberian continental margin: Insights from preserved submarine palaeotopography in the Longobucco Basin (Calabria, Southern Italy). *Sedimentary Geology*, 331, 94–113. <https://doi.org/10.1016/j.sedgeo.2015.10.010>
- Santorò, E., Mazzella, M. E., Ferranti, L., Randisi, A., Napolitano, E., Rittner, S., & Radtke, U. (2009). Raised coastal terraces along the Ionian Sea coast of northern Calabria, Italy, suggest space and time variability of tectonic uplift rates. *Quaternary International*, 206(1–2), 78–101. <https://doi.org/10.1016/j.quaint.2008.10.003>
- Scandone, P. (1979). Origin of the Tyrrhenian Sea and Calabrian arc. *Bollettino della Società Geologica Italiana*, 98, 27–34.
- Schiattarella, M. (1998). Quaternary tectonics of the Pollino Ridge, Calabria-Lucania boundary, southern Italy. *Geological Society, London, Special Publications*, 135(1), 341–354. <https://doi.org/10.1144/gsl.sp.1998.135.01.22>
- Schiattarella, M., Giano, S. I., & Gioia, D. (2017). Long-term geomorphological evolution of the axial zone of the Campania-Lucania Apennine, southern Italy: A review. *Geologica Carpathica*, 68(1), 57–67. <https://doi.org/10.1515/geoca-2017-0005>
- Schiattarella, M., di Leo, P., Beneduce, P., & Giano, S. I. (2003). Quaternary uplift vs tectonic loading: A case study from the Lucanian Apennine, southern Italy. *Quaternary International*, 101–102, 239–251. [https://doi.org/10.1016/S1040-6182\(02\)00126-X](https://doi.org/10.1016/S1040-6182(02)00126-X)
- Schiattarella, M., Torrente, M., & Russo, F. (1994). Analisi strutturale ed osservazioni morfostratigrafiche nel bacino del Mercure (confine calabro-lucano). *Il Quaternario*, 7, 613–626.
- Schildgen, T. F., Cosentino, D., Caruso, A., Buchwaldt, R., Yldrm, C., Bowring, S. A., et al. (2012). Surface expression of eastern Mediterranean slab dynamics: Neogene topographic and structural evolution of the southwest margin of the Central Anatolian Plateau, Turkey. *Tectonics*, 31(2). <https://doi.org/10.1029/2011TC003021>
- Schwanghart, W., & Scherler, D. (2014). Short communication: TopoToolbox 2 – MATLAB-based software for topographic analysis and modeling in Earth surface sciences. *Earth Surface Dynamics*, 2(1), 1–7. <https://doi.org/10.5194/esurf-2-1-2014>
- Servizio Geologico d'Italia. (1971). 221 Castrovillari sheet of the Carta Geologica D'Italia, 1: 100,000 scale.
- Siravo, G., Speranza, F., & Macri, P. (2022). First pre-miocene paleomagnetic data from the calabrian block document a 160° post-late jurassic CCW rotation as a consequence of left-lateral shear along Alpine tethys. *Tectonics*, 41(7), e2021TC007156. <https://doi.org/10.1029/2021TC007156>
- Spina, V., Tondi, E., & Mazzoli, S. (2011). Complex basin development in a wrench-dominated back-arc area: Tectonic evolution of the Crati Basin, Calabria, Italy. *Journal of Geodynamics*, 51(2–3), 90–109. <https://doi.org/10.1016/j.jog.2010.05.003>
- Stock, J. D., & Montgomery, D. R. (1999). Geologic constraints on bedrock river incision using the stream power law. *Journal of Geophysical Research*, 104(B3), 4983–4993. <https://doi.org/10.1029/98JB02139>
- Struth, L., Garcia-Castellanos, D., Viaplana-Muzas, M., & Vergés, J. (2019). Drainage network dynamics and knickpoint evolution in the Ebro and Duero basins: From endorheism to exorheism. *Geomorphology*, 327, 554–571. <https://doi.org/10.1016/j.geomorph.2018.11.033>
- Tarquini, S., Vinci, S., Favalli, M., Doumaz, F., Fornaciai, A., & Nannipieri, L. (2012). Release of a 10-m-resolution DEM for the Italian territory: Comparison with global-coverage DEMs and anaglyph-mode exploration via the web. *Computers & Geosciences*, 38(1), 168–170. <https://doi.org/10.1016/j.cageo.2011.04.018>
- Tofelde, S., Savi, S., Wickert, A. D., Bufo, A., & Schildgen, T. F. (2019). Alluvial channel response to environmental perturbations: Fill-terrace formation and sediment-signal disruption. *Earth Surface Dynamics*, 7(2), 609–631. <https://doi.org/10.5194/esurf-7-609-2019>
- Tropeano, M., Sabato, L., & Pieri, P. (2002). Filling and cannibalization of a foredeep: The Bradanic Trough, Southern Italy. *Geological Society, London, Special Publications*, 191(1), 55–79. <https://doi.org/10.1144/GSL.SP.2002.191.01.05>
- Vandenbergh, J. (1995). Timescales, climate and river development. *Quaternary Science Reviews*, 14(6), 631–638. [https://doi.org/10.1016/0277-3791\(95\)00043-0](https://doi.org/10.1016/0277-3791(95)00043-0)
- Van Dijk, J. P., Bello, M., Brancaleoni, G., Cantarella, G., Costa, V., Frixia, A., et al. (2000). A regional structural model for the northern sector of the Calabrian Arc (southern Italy). *Tectonophysics*, 324(4), 267–320. [https://doi.org/10.1016/S0040-1951\(00\)00139-6](https://doi.org/10.1016/S0040-1951(00)00139-6)
- Vignaroli, G., Minelli, L., Rossetti, F., Balestrieri, M. L., & Faccenna, C. (2012). Miocene thrusting in the eastern Sila Massif: Implication for the evolution of the Calabria-Peloritani orogenic wedge (southern Italy). *Tectonophysics*, 538, 105–119. <https://doi.org/10.1016/j.tecto.2012.03.011>
- Whipple, K. X., & Tucker, G. E. (1999). Dynamics of the stream-power river incision model: Implications for height limits of mountain ranges, landscape response timescales, and research needs. *Journal of Geophysical Research*, 104(B8), 17661–17674. <https://doi.org/10.1029/1999jb900120>
- Willett, S. D., McCoy, S. W., Perron, J. T., Goren, L., & Chen, C. Y. (2014). Dynamic reorganization of river basins. *Science*, 343(6175), 1248765. <https://doi.org/10.1126/science.1248765>
- Willett, S. D., Slingerland, R., & Hovius, N. (2001). Uplift, shortening, and steady state topography in active mountain belts. *American Journal of Science*, 301(4–5), 455–485. <https://doi.org/10.2475/ajs.301.4-5.455>
- Wobus, C., Whipple, K. X., Kirby, E., Snyder, N., Johnson, J., Spyropoulos, K., et al. (2006). Tectonics from topography: Procedures, promise, and pitfalls. *Special Papers - Geological Society of America*, 398, 55–74. [https://doi.org/10.1130/2006.2398\(04](https://doi.org/10.1130/2006.2398(04)
- Wortel, M. J. R., & Spakman, W. (2000). Subduction and slab detachment in the Mediterranean-Carpathian region. *Science*, 290(5498), 1910–1917. <https://doi.org/10.1126/science.290.5498.1910>
- Zecchin, M., Accaino, F., Ceramicola, S., Civile, D., Critelli, S., da Lio, C., et al. (2018). The Crotona Megalandslide, southern Italy: Architecture, timing and tectonic control. *Scientific Reports*, 8(1), 7778. <https://doi.org/10.1038/s41598-018-26266-y>